Fracture initiation in ductile metals*

P. Rama Rao

Defence Research and Development Organization, Room No. 156, B-Wing, Sena Bhavan, New Delhi 110 011, India

A major research and development programme that began more than a decade ago and is still underway at the Defence Metallurgical Research Laboratory seeks to, on the one hand, investigate certain aspects of ductile fracture in iron and binary iron solid solution alloys and, on the other, develop a suitable low alloy ultra-high strength (yield strength better than 1500 Mpa) steel with relatively high fracture toughness (fracture toughness better than 80 Mpa$\sqrt{m}$). Fracture toughness measurements were carried out on Armco Fe with varying grain size and at different temperatures and on a whole series of iron alloys: Fe-Si, Fe-Mo, Fe-Ni, Fe-Co, Fe-Cr, Fe-C, Fe-C-Ni, Fe-C-Co, Fe-C-Ni-Si-Cr, Fe-C-Ni-Si-Cr-Co, Fe-C-Ni-Si-Cr-Mo and Fe-C-Ni-Si-Cr-Mo-Co. Through scanning electron metallography, measurements have been made of the characteristic distance of the void ahead of the blunted crack tip and the stretch zone width to determine the crack tip opening displacement. Using an approach involving these measurements and the plastic flow related energy dissipation in the HRR (Hutchinson–Rice–Rosengren) zone beyond the process zone and the calculation of J_{Ic} in terms of the critical strain model originally developed by Rice and Johnson and Ritchie and Thompson, it is shown that measured J_{Ic} covering a wide range (100–300 kJ/m^2) can be estimated. The NiSiCrMoCo steel has been now produced on tonnage scale at MIDHANI, Hyderabad. Following the development of welding consumables and evaluation of the weld joint efficiencies, the use of this structural steel for high technology applications is currently under progress.

In the world of materials the dominant fraction (~ 95%) by weight is accounted for by engineering materials. The balance belongs to the so-called functional materials which perform critical functions in various modern devices like the computers and other electronic systems and these are currently receiving the bulk of research attention and funding. About 70% of the engineering materials, by weight again, would be metals and alloys, although this proportion is diminishing with polymers and composites registering high growth rates. Steels, the work horse of the engineering materials, are the material of interest in the present article, and these account for about 80% of the metals produced and, thus, for more than half of all of the materials.

Engineering materials are used in load-bearing applications where reliability and durability are governed by the three engineering properties, viz. Young's modulus, yield strength and fracture toughness. Failure of structural parts can be caused by buckling when they are not stiff enough, or by plastic yielding when resistance to plastic deformation is not adequate or by fracture when there is collapse of resistance to crack propagation. Failure criteria of a structural member in the three situations would be respectively dictated by Young's modulus, yield strength and fracture toughness.

Let us take stock of these properties in the various types of solids. Metals are inherently weak solids – yield strength of Fe single crystals is as low as 28 MPa. Compare this with the strength of diamond, which is 10,000 MPa. Polymers are floppy kind of solids and so they are low-modulus materials. Compare the value of E for polyethylene (0.15 GPa) with that of diamond (1000 GPa). Ceramics are naturally brittle solids – fracture toughness value of 3 MPa$\sqrt{m}$ for alumina may be compared with 200 MPa$\sqrt{m}$ for mild steel. Most of engineering materials science is dedicated to combat the inherent weakness in each class. The result is strong steels (e.g. piano wire with an yield strength of 2750 MPa), engineering plastics (e.g. melamine with a modulus of ~ 9 GPa) and tough ceramics (e.g. cermet with fracture toughness of ~ 20 MPa$\sqrt{m}$). The most successful and consistent achievement is in respect of strengthening metals and the more challenging has been to enhance fracture toughness of ceramics. Fracture toughness of < 15 MPa$\sqrt{m}$ is generally unacceptable in an engineering structure and it is this aspect which has hitherto hindered the use of ceramics in load-bearing applications. We will be concerned with fracture toughness in this article, although not in respect of ceramics or, for that matter, brittle solids.

The focus of this article is on fracture. Fundamentally there are only two fracture modes – brittle and ductile. Cleavage fracture is an instance of brittle failure which takes place by breaking atomic bonds across cleavage planes. Failure of ductile solids can also occur in the brittle mode as happens in iron (cleavage) at low temperatures, below what has been termed the ductile–brittle transition temperature. Brittle fracture has been studied extensively and is not dealt with here. We will turn our attention to ductile fracture, a three-step process involving formation of a void, its growth due to plastic deformation of the surrounding ductile material and then, once the void has grown beyond a certain size usually

*Text of President's address delivered at the 61st Annual Meeting of the Indian Academy of Sciences held at Madras, 10 November 1995.

expressed in terms of the distance of separation between neighbouring voids, the ligament failure causing void linkage resulting in the formation of a crack that will propagate catastrophically. The problem becomes more complex when one has to analyse the effects of high temperature (creep fracture) or of chemical attack (stress corrosion).

Milestones in fracture theory

The analysis of fracture progressed as the understanding of material behaviour was combined with the principles of mechanics and the way this subject developed thereby is an outstanding instance of interdisciplinary approach successfully contributing to the blossoming of a field of research.

The quantitative relations that engineers and scientists use today in determining the fracture of cracked solids were initially stated 75 years ago by Griffith[1]. He noted that fracture takes place when the strain energy that is released by extending a crack exceeds the surface energy, γ_s, required to form the extra crack surface.

$$\sigma_f = \left(\frac{2E\gamma_s}{\Pi a(1-\nu^2)} \right)^{1/2}, \tag{1}$$

where σ_f is the fracture stress, γ the Poisson's ratio and a the crack length. Griffith worked on glass and to deal with metals in a similar way Orowan[2] and Irwin[3] independently suggested that we add to the surface energy term the energy associated with the plastic deformation (γ_p) in the fracture process, i.e. γ_s in equation (1) becomes $\gamma_p + \gamma_s$. Mott[4] extended the Griffith theory to *rapidly* propagating cracks.

Subsequently Irwin and Kies[5] showed that, for a single crack tip, the strain energy release rate per unit thickness (dU_e/da) is given in terms of load and compliance, and then they related this to Griffith's strain energy release rate designated as G, i.e.

$$\frac{dU_e}{da} = \frac{P^2}{2}\frac{dC}{da} = G, \tag{2}$$

where P is the applied force and C the elastic compliance per unit thickness. *This relationship has made a significant contribution to fracture mechanics since it can be applied to any geometry subjected to elastic loading.*

The next major advance, regarded as a turning point, occurred when Irwin[6] showed that stresses and displacements near the crack tip can be related through a single parameter K that in turn was related to the strain energy release rate G. With reference to Figure 1 the parameter K is the stress intensity factor

$$\sigma_{ij} = \frac{K}{2\pi r} f_i(\theta). \tag{3}$$

Imagining that crack extended by an amount Δa, Irwin calculated the work required to close it back up to its original length. This amount of work can be equated to the product of the energy release rate and the crack extension increment. Thus

$$G\Delta a = 2\int_a^{a+\Delta a} (\tfrac{1}{2}\sigma_{yy}(x)v(x-\Delta a)\,dx). \tag{4}$$

Or, upon substituting

$$\sigma_{yy} \approx K[2\pi(x-a)]^{-1/2}, \qquad x > a$$

$$v \approx \frac{(1+\nu)(\kappa+1)}{E} K \left(\frac{a-x}{2\pi} \right)^{1/2}, \quad x < a.$$

Irwin obtained

$$G = \tfrac{1}{4}(1+\nu)(\kappa+1)\frac{K^2}{E} = \frac{K^2}{E'}, \tag{5}$$

where $E' = E$ for plane stress and $E' = E/(1-\nu^2)$ for plane strain.

Presently we are concerned with ductile metals, which exhibit considerable plastic yield, for which the stress

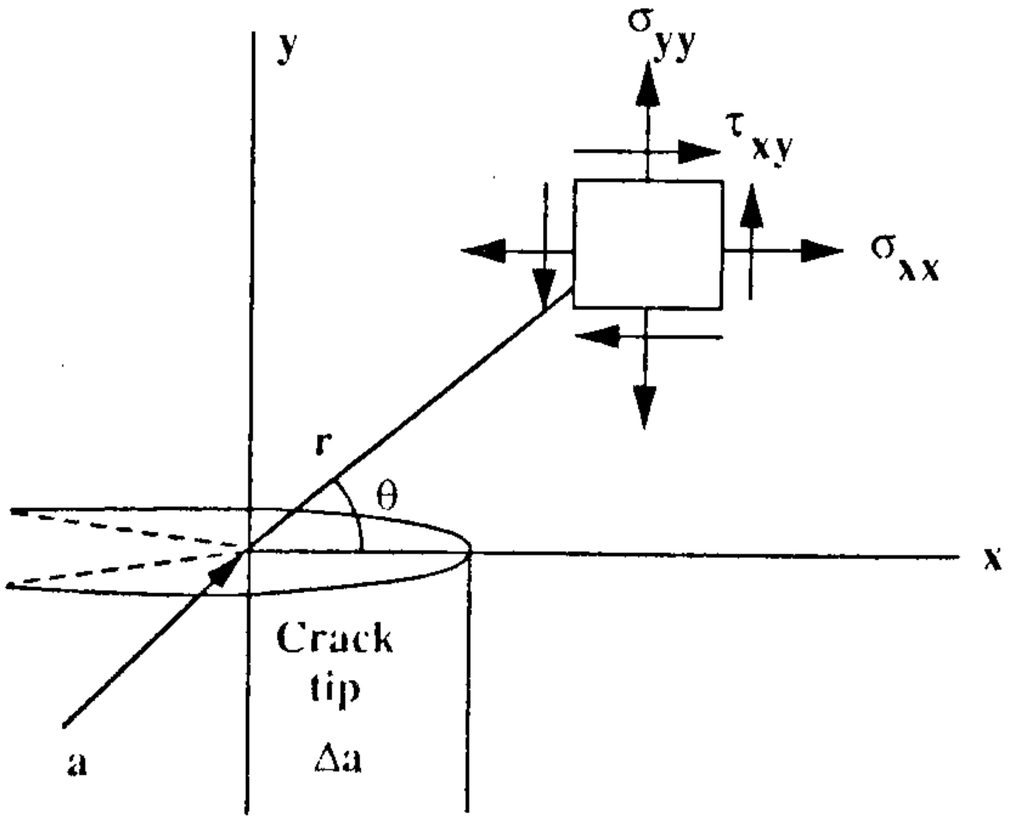

Figure 1. Coordinates used to describe stresses near a crack tip.

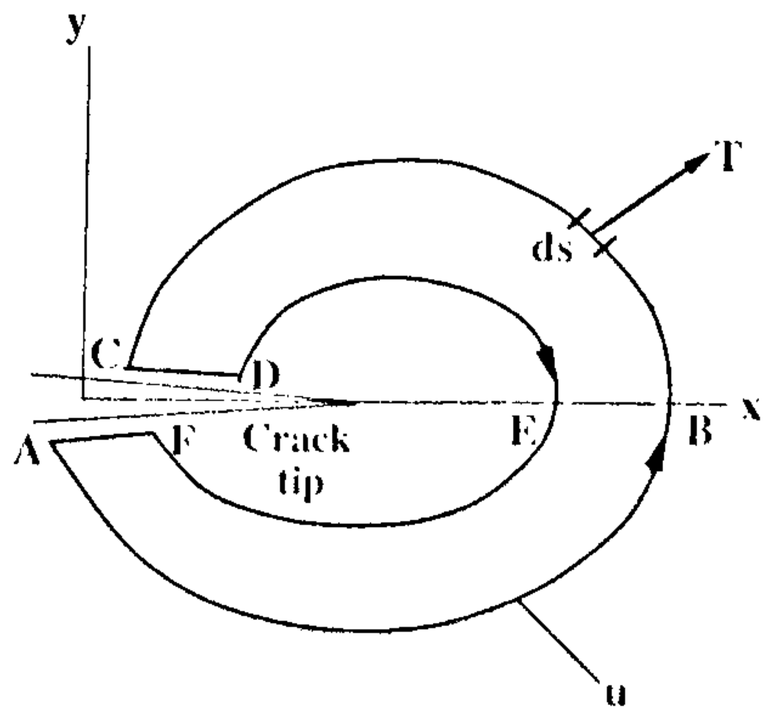

Figure 2. Path independent J integral.

and strain relation is not elastic. For these, the strength of stress and displacement fields near a crack tip were characterized by a parameter called J by Rice[7], keeping in view that the exponents of stress and strain must reflect the functional relationship between the stress and strain implied by the nonlinear stress–strain curve appropriate to ductile solids. J of Rice extended Irwin's strain energy release rate to encompass nonlinear behaviour, as well as his virtual work treatment outlined above to treat a general contour around the crack tip starting from the lower crack face, including the singularity and terminating on the upper surface. The J integral around any such contour incorporating stored energy density and tractions on the contour have been shown to be *path independent* (Figure 2). The J integral can be written in the form

$$J = \int \left[\sigma\varepsilon \, dy - \boldsymbol{T} \frac{\partial \boldsymbol{u}}{\partial x} ds \right], \qquad (6)$$

where $\sigma\varepsilon$ is the strain energy density, s the path of the integral which encloses the crack, $\boldsymbol{T}$ the outward traction vector acting on the contour around the crack, $\boldsymbol{u}$ the displacement vector and ds the length increment along the contour. Since J is path independent, one may choose the most convenient path, usually the specimen boundary. One can again postulate that the crack growth occurs if J exceeds the critical value J_{Ic}. For the case of linear elastic material,

$$J_{Ic} = G_{Ic} = K_{Ic}^2 / E' , \qquad (7)$$

where suffix I stands for tensile mode of loading.

Rice's work might have been relegated to obscurity had it not been for the demanding research effort of the nuclear power industry driven by legitimate concerns for safety, as well as political and public relations considerations. In 1972, Begley and Landes[8] conducted experiments to determine the fracture toughness properties of steels and their successful experiments led to the publication of a standard procedure for J testing of metals ten years later.

Table 1. Strengthening mechanisms

Mechanism	Relation
Dislocation	$\Delta\sigma \approx \alpha G b \sqrt{\rho}$
Grain size	$\Delta\sigma \approx \Delta\sigma_0 + k/d^{1/2}$
Solid solution	$\Delta\sigma \approx A\,(\varepsilon_s)^{3/2}\, C^{1/2}$
Precipitation and dispersion	$\Delta\sigma \approx \beta G b/\lambda$
Multiphase	$\Delta\sigma \approx f\,(\sigma_{II}, \sigma_I)$

G = Shear modulus; ρ = Dislocation density; b = Burger's vector; d = grain size; C = Concentration of solute; λ = Interparticle/dispersoid distance; σ = Yield strength; ε_s = Lattice misfit strain; A, β = Constants.

Alloy development

Alloy development calls for not only improvement of strength but also enhancement in fracture resistance. In regard to strengthening, a large experimental data bank has become available alongside impressive theoretical treatments. As a result, strengthening due to various mechanisms has been quantitatively predicted and validated (Table 1). Using this knowledge base it has been demonstrated that it is possible to *design* industrial alloys (e.g. high-strength low-alloy steels) to meet the desired strength levels[9]. With regard to fracture resistance, we did not have for long an equivalent level of understanding. The problem of fracture toughness needed to be addressed, because the more the strength is built into a given material, the more prone to brittle fracture it becomes (Figure 3). If we have to develop strong *as well as tough alloys*, we must find methods by which the yield strength–fracture toughness strength plot in Figure 3 is displaced outward diagonally as shown. This has indeed been the endeavour in the case of steels marked by the development of ultrahigh strength, high fracture toughness steels like the maraging steel[10]. In the event, substantial understanding has emerged about the way microstructural features respond to fracture processes, particularly in the regime of multiphase engineering alloys strengthened by the presence of particles – carbides in structural steels and intermetallic precipitates in alloy steels such as maraging steel.

Single phase and relatively cleaner alloys would have been excellent model materials to work with (as shown by research on strengthening mechanisms) for generating basic understanding of ductile fracture; but this has remained substantially unattended. This is the niche area chosen for ductile fracture research at DMRL with the following goals: (i) generate experimental data, which is the difficult aspect as the materials are ductile, (ii) relate to ductile fracture theory, and (iii) use the information alongside that available in the literature to develop a new composition for an ultrahigh strength, high fracture

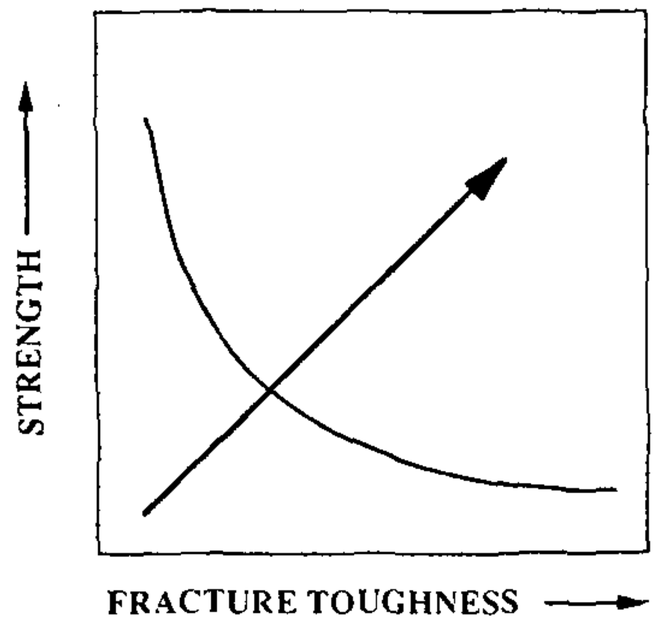

Figure 3. A schematic diagram showing variation of strength with fracture toughness.

ıghness *low-alloy steel*, and (iv) develop the same ough industrial processing for engineering applications.

easuring fracture toughness

pointed out earlier, J_{Ic} is the appropriate measure fracture toughness of ductile metals. What perhaps ; deterred carrying out measurements of fracture tough- ;s J_{Ic} of very ductile solids such as purer metals and gle phase binary alloys is the enormity of the needed ort arising out of the specimen dimensions for valid ests[11]. The validity criterion to be fulfilled stipulates t the thickness of the specimen (B) for a valid test should exceed a minimum value defined by $B > 25J_{Ic}/\sigma_{yt}$, where σ_{yt} is the average of yield and tensile strength. Since we are dealing with high J_{Ic} and low σ_{yt}, on account of our test materials being single phase materials which are soft, the specimen thicknesses are rather large. A standard compact tension specimen would be of 50 mm thickness weighing around 6.0 kg as compared to a tensile specimen (for strength measurement) that weighs less than 100 g. Further, the fracture toughness specimens are of more complicated geometry (Figure 4) and are, therefore, more difficult to machine.

The J_{Ic} measurement technique[11] involves measurement of the area under load–displacement plot, obtained from notched and precracked specimens and the corresponding crack extension Δa (Figure 5). To obtain a single value of J_{Ic}, 4 to 6 specimens are to be tested. (The elastic unloading-based single specimen technique could not be employed due to considerable crack tip plasticity[12]). In the case of strongly hardening metals, as in the present instance, ASTM[11]-suggested theoretical blunting line was inapplicable. It therefore became necessary to establish experimentally the blunting line, corresponding to the initial extension of the crack due to crack tip blunting[12,13]. For this purpose scanning electron fractography was used to measure what is referred to as the width of the stretched zone, which refers actually to the stretch of the crack as a consequence of blunting. The complete details of the test procedure are available in Srinivas *et al.*[12].

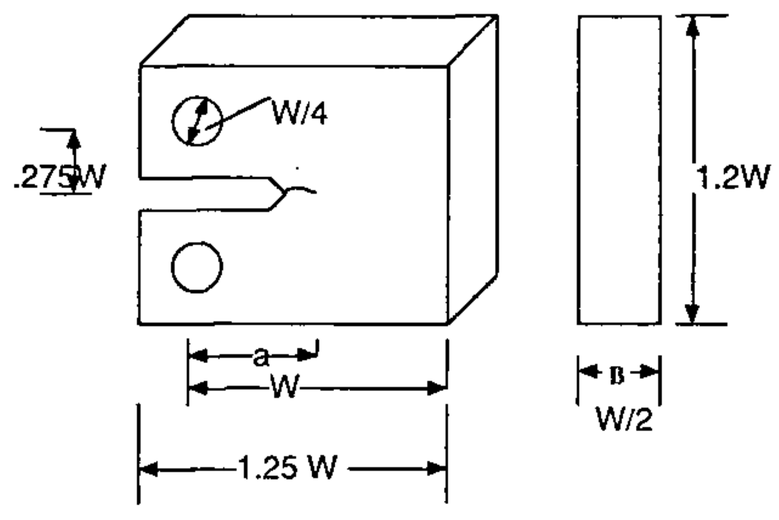

Figure 4. Specimen geometries for fracture toughness testing.

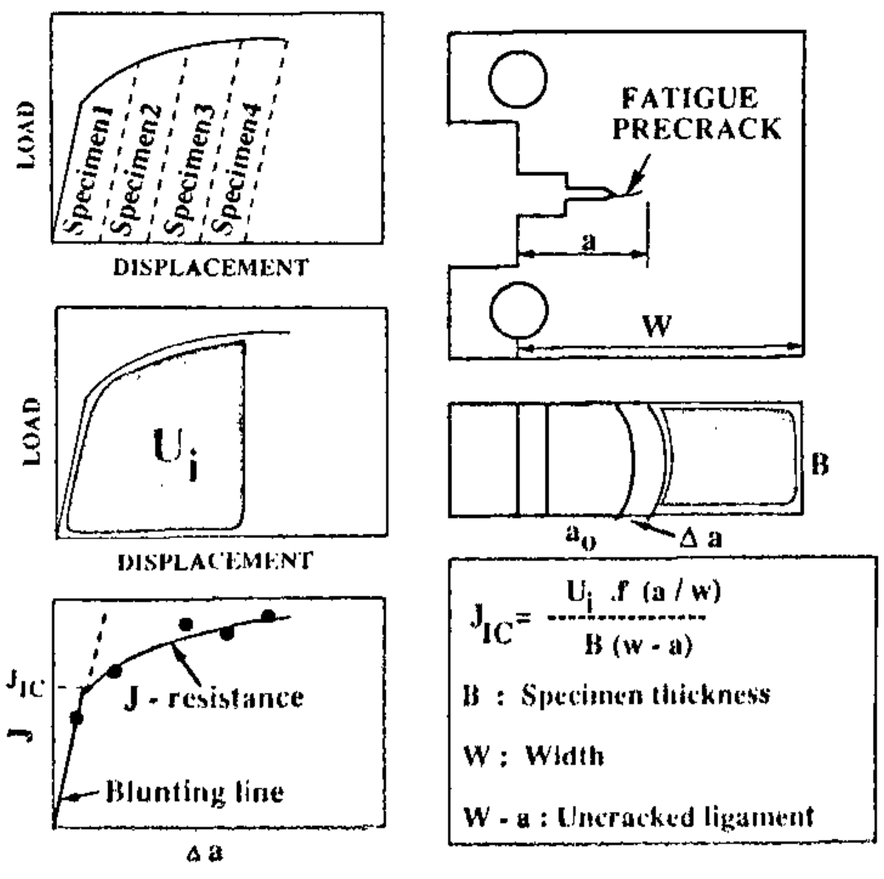

Figure 5. Test method for J_{Ic}

The ductile fracture process

The basic objective of any theoretical treatment would be to arrive at expressions, in terms of measurable parameters, based on an analysis of the crack extension process, with the help of which the value of J can be predicted. By and large, till now, only the effects of loading and geometry are considered. The scale of consideration would correspond to, at best, the macro scale with hardly any attention to features at finer scale within the plastic zone. This is to be contrasted with the interest of physicists which would be at the atomic level. The physics of crack extension at the atomic level would consider ion and electron cloud configurations involved in the crack extension process, analyse the same from wave mechanics and integrate the results[14]. The magnitude of the problem may be gauged from the fact that in the case of crack extension, integration dauntingly would have to be over ten orders of magnitude. This seems intractable. The work that we present here is therefore to be content with just the size of the plastic zone and making measurements related to micro scale features within the plastic zone.

The sequence of events leading to crack initiation during ductile failure (Figure 6) is as follows: (a) blunting of the sharp crack, (b) nucleation of a void at

a characteristic distance l_c from the crack tip, (c) growth of the void due to plastic flow under triaxial tensile stress conditions, and (d) coalescence of the void with the main crack resulting in crack initiation (plastic collapse). Initiation fracture toughness J_{Ic}, where the suffix *I* suggests uniaxial tensile mode of loading, corresponds to the event, (d) the strain hardening characteristic

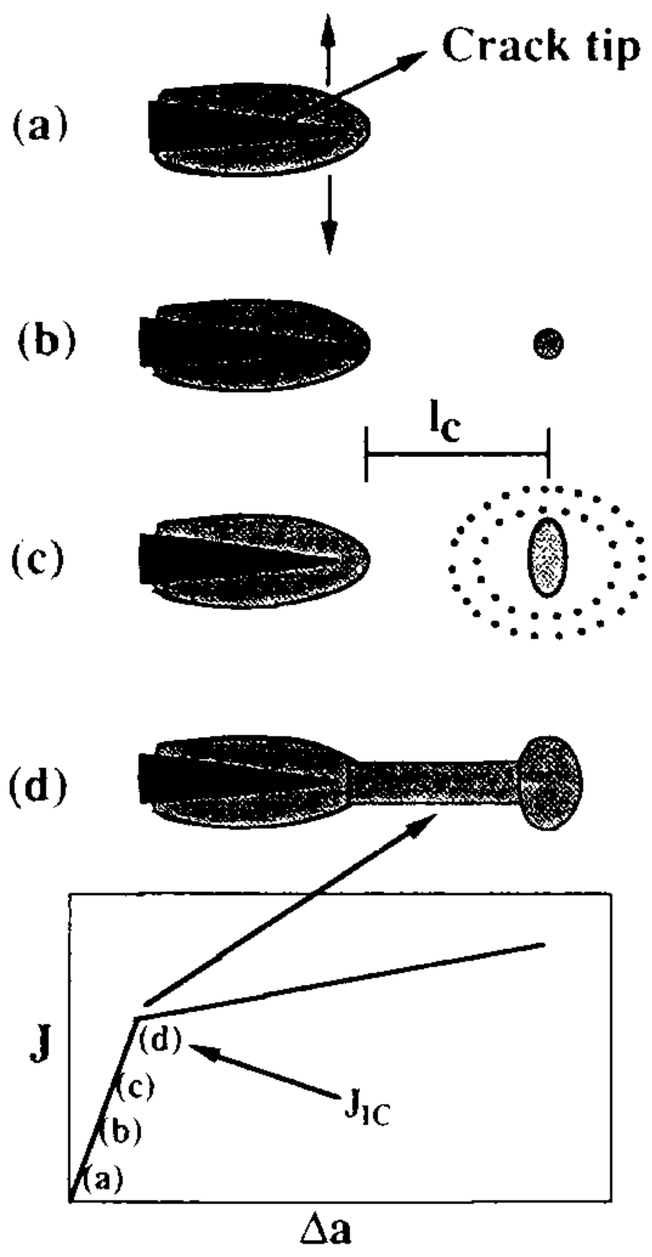

Figure 6. Sequence of events leading to crack initiation during ductile failure.

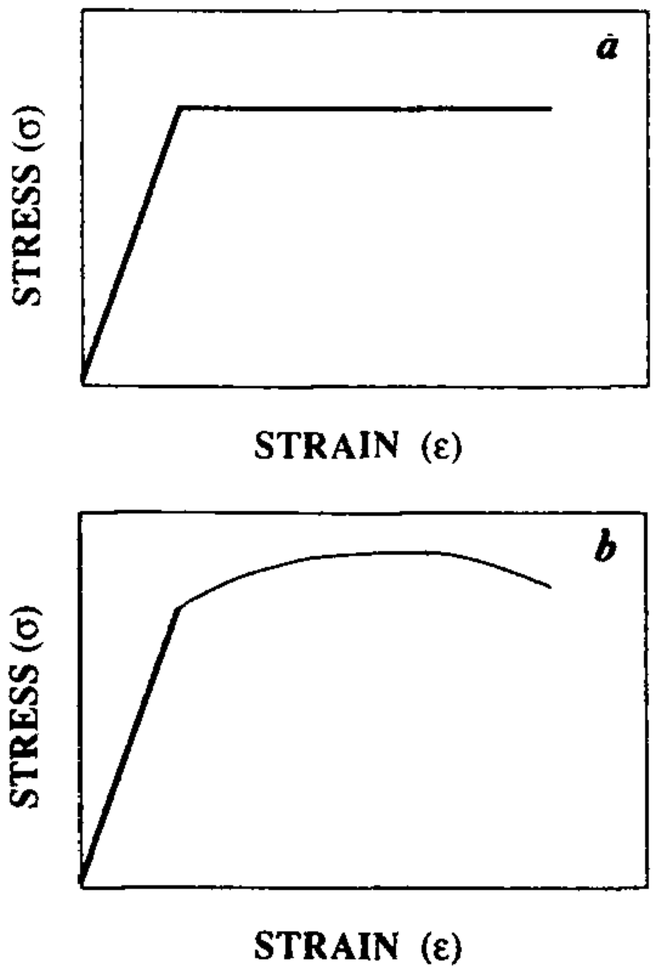

Figure 7. Schematic stress–strain curves for (*a*) non-hardening material and (*b*) strain-hardening material.

of the material influences the void nucleation and growth processes.

A criterion for crack initiation

For fracture to initiate, critical strain has to be exceeded over the characteristic distance, l_c. The use of the characteristic distance has been importantly resorted to[15–19] in the evaluation of J_{Ic}. The initiation fracture toughness J_{Ic} is nearly equal to the product of plastic work per unit volume and the characteristic distance l_c. For a nonhardening material, the forms of the stress (σ) and strain (ε) relation would be of the form shown in Figure 7 *a* and

$$J_{Ic} = (\sigma_f \varepsilon_f) l_c . \tag{8}$$

For a strain hardening ($\sigma = K_H \varepsilon^n$) material (Figure 7 *b*),

$$J_{Ic} \simeq [\int \sigma \, d\varepsilon \,] \varepsilon_f . l_c .$$
$$\simeq \{(K_H \varepsilon_f)^{n+1}/n + 1\} l_c . \tag{9}$$

Evaluation of J_{Ic} thus requires the knowledge of the characteristic distance l_c, the critical fracture strain ε_{fr} to be exceeded over the characteristic distance and the strain hardening exponent *n*.

The critical distance l_c arises from the net result of the variation of the strain (ε) and hydrostatic stress (tensile), σ_m, ahead of the crack[20]. From the strain variation, the local flow stress (σ_{flow}) can be calculated from $\sigma_{flow} = K_H \varepsilon^n$. For void nucleation to occur, $\sigma_m + \sigma_{flow}$ should exceed a critical stress σ_c. $\sigma_m + \sigma_{flow}$ will attain a maximum value neither at the crack tip (because σ_m is low at the crack tip) nor at a distance greater than a few times the crack tip opening displacement δ_t (because strain becomes too low), but at some intermediate distance (Figure 8).

The characteristic distance has been commonly used in the evaluation of J_{Ic} whether it is the stress- or strain-based approach to determine the failure criteria.

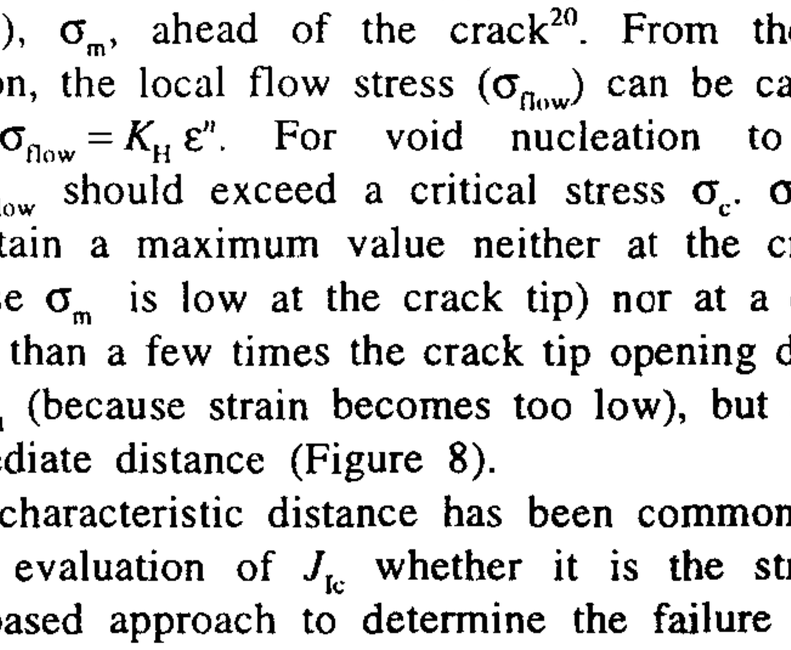

Figure 8. Stress distribution ahead of a blunted crack tip.

Various values have been assigned to l_c which has been conceived to be microstructure-dependent (Table 2). However, no direct measurement of l_c seems to have been made so far. This is partly attributable to the type of materials invariably investigated, namely particle containing (e.g. carbide-strengthened steels) materials.

Void nucleation in particle-bearing materials occurs by interface decohesion or by particle cracking (Figure 9). On the other hand, in particle-free materials, such as Armco iron under consideration, void nucleation mechanism is deformation related and occurs by slip band intersection or slip band impingement on grain boundary (Figure 9) which has been measured by us as described below.

Scanning electron metallographic measurements

Void nucleation

For direct observation of void nucleation and measurement of l_c, the material chosen is Armco iron which was essentially particle-free in the sense that no particles were resolved at the optical level. High resolution electron microscopy revealed particles too small to be considered responsible (below the size suggested by Argon *et al.*[21]) for void nucleation at them. Evidence was obtained for the nucleation of voids at slip band intersection and at sites where slip band impingement on grain boundaries occurred (Figure 10).

Table 2. Characteristic distance vs microstructural constituent

Model	Relation
Ritchie, Knott and Rice[37]	$l_c \approx 2 \times$ grain size
Curry[38]; Knott[20]	$l_c \approx$ inter-particle distance
Garrison[15], Ritchie and Thompson[19], Rice and Johnson[29]	$l_c \approx$ mean spacing of the void nucleating large particles
Lin, Evans and Ritchie[16,17,31]	$l_c \approx$ distance based on statistical approach

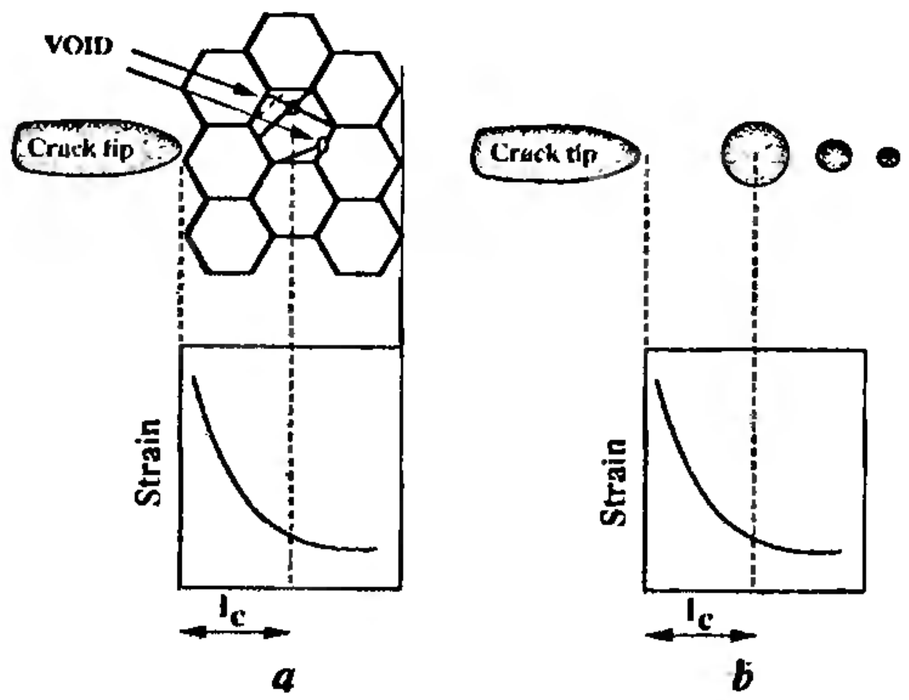

Figure 9. Void nucleation in (*a*) particle-free and (*b*) particle-containing materials.

Characteristic distance l_c

With the objective of determining the void site ahead of the crack tip, the compact tension toughness test of Armco iron (38 μm grain size) was interrupted at regular displacement intervals, samples mid-sectioned, polished, etched and examined. An SEM micrograph corresponding to the displacement level of 2.9 mm is shown in Figure 11. At this displacement, the crack tip had blunted extensively and developed a nearly semicircular profile. Figure 11 reveals formation of voids ahead of the blunted crack tip. These voids form a semicircular array parallel to the blunted crack tip profile. The distance between the first parallel void array and the crack tip is 125 μm. The diminishing void size as one moves away from the crack plane recorded in the case of 78 μm grain size Armco iron (Figure 12) is a reflection of the HRR strain field variation, ahead of the blunted crack, given by the expression[22,23]

$$\varepsilon_{ij}(X,\theta) = (J/K_H I_n X)^{1/n+1}\, \varepsilon_{ij}(\theta,n)\,, \qquad (10)$$

where J represents the J-integral value, I_n is a constant which depends on n, X is the distance ahead of the crack tip, θ is the angle from the plane of the crack and $\varepsilon_{ij}(\theta,n)$ is a normalizing function to account for the variation in the strain profile with angle θ.

That l_c is indeed a microstructure-dependent parameter is brought out by observations similarly made when the microstructural parameter grain size was varied in iron (Figure 13). l_c measurements show that with increasing grain size l_c decreases.

INTERSECTION OF SLIP BANDS

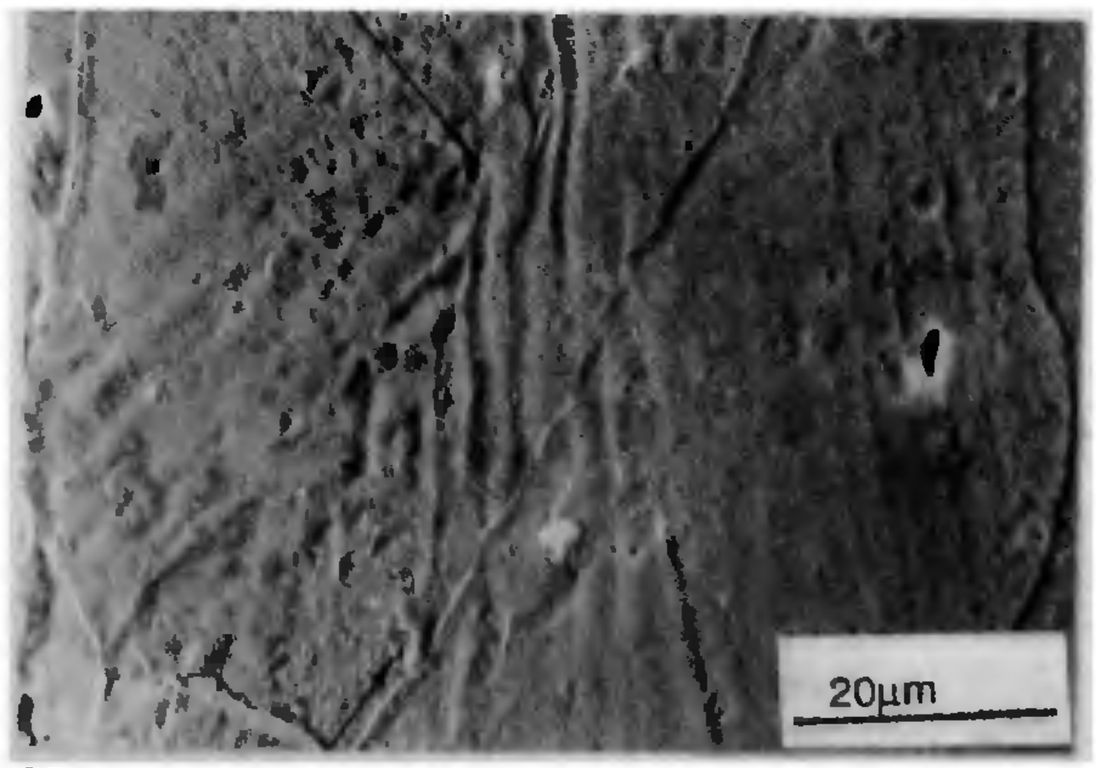

SLIP BAND IMPINGEMENT ON GRAIN BOUNDARY

Figure 10. Scanning electron micrograph showing the nucleation of voids by slip band impingement: mutual intersection of slip bands and intersection with the grain boundary.

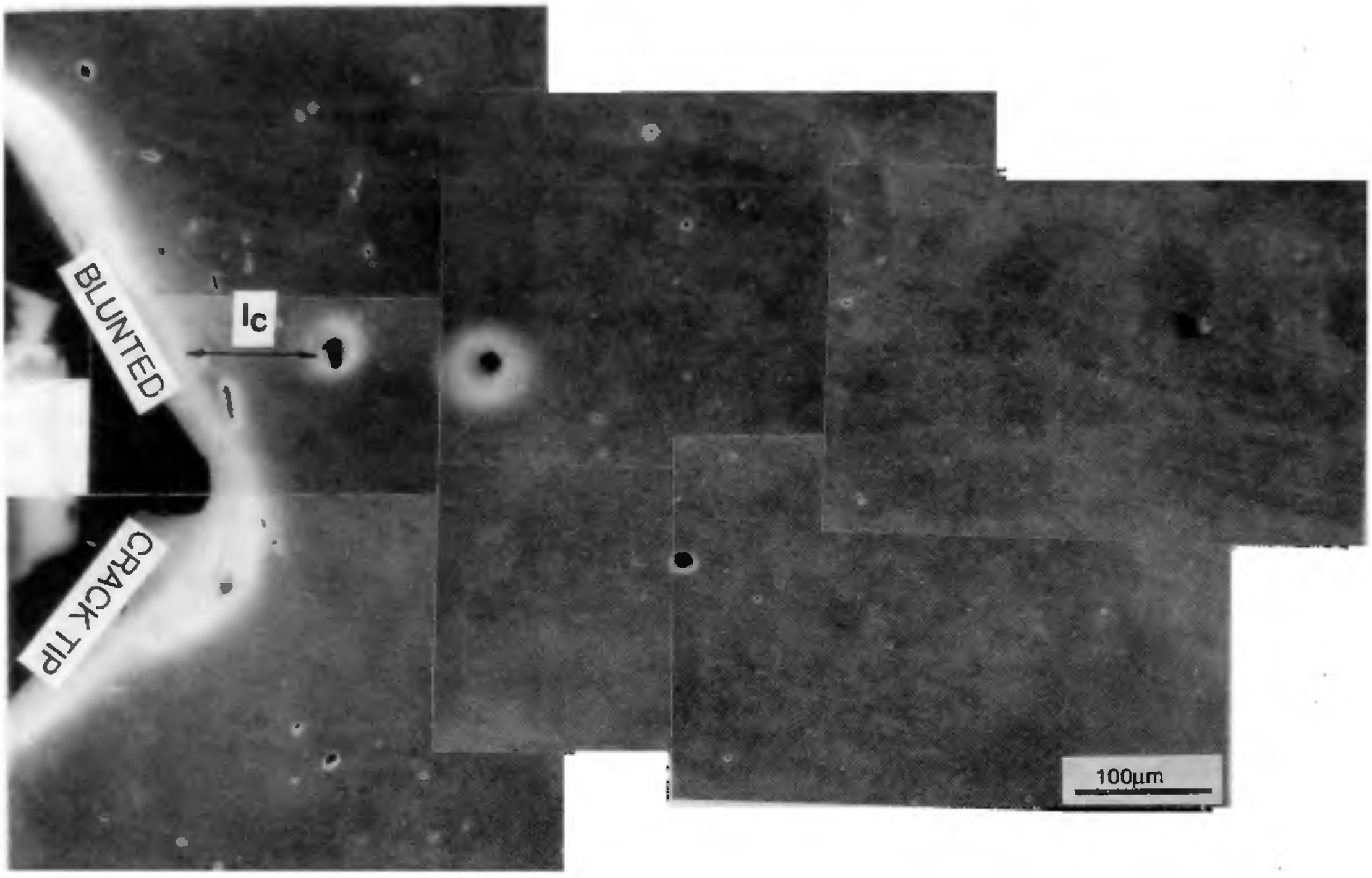

Figure 11. Scanning electron micrographs of Armco iron of 38 µm grain size corresponding to a displacement level of 2.9 mm in an interrupted fracture toughness test.

Stretch zone width

The stretch zone is a featureless zone between the fatigue precracked region and the point of onset of stable crack growth. The stretch zone width (SZW) increases with displacement during loading and attains a critical value (SZW_c), beyond which stable crack growth commences. SZW measurements were carried out to establish the experimental blunting line and to derive J_{Ic} from the critical value SZW_c. Scanning electron fractographs revealing the stretch zone width (SZW) for Fe and Fe–5Co are shown in Figure 14. The toughening effect of cobalt on iron is manifest in the enhanced SZW for Fe–5Co material.

The SZW measurements served yet another purpose. The crack opening displacement is relatable to SZW[24] and is equal to twice SZW (Figure 14). Through SZW measurements the critical crack tip opening displacement δ_{tc} can therefore be estimated. This is of much value as the relationship between l_c and δ_{tc} is needed in the ductile fracture analysis.

l_c *vs grain size and* δ_{tc}

As mentioned earlier, l_c measurements were made as a function of grain size. Grain size influences fracture toughness and thereby δ_{tc}. The consequent variation of δ_{Ic} with l_c was found to be linear (Figure 15) and could be expressed as $l_c = 0.315\,\delta_{tc}$. Since δ_{tc} is twice SZW, this expression enables estimation of l_c from SZW measurements.

Measurement of J_{Ic}

If our understanding of the ductile fracture features observed and measured through scanning electron metallography has to be placed on a more sound footing, we need substantial quantitative measurements of J_{Ic}. This was undertaken in respect of Armco iron. For this purpose three important variables, viz. grain size, solute additions and test temperature were chosen. Studies on each of these variables, as will be seen below, not only yielded a wide range of J_{Ic} values (100–300 kJ/m^2) but also significant new observations.

Grain size effects

The influence of grain size on the strength of metals and alloys is well established in terms of the well-known Hall–Petch relationship

$$\sigma_y = \sigma_0 + k_y/d^{1/2}, \qquad (11)$$

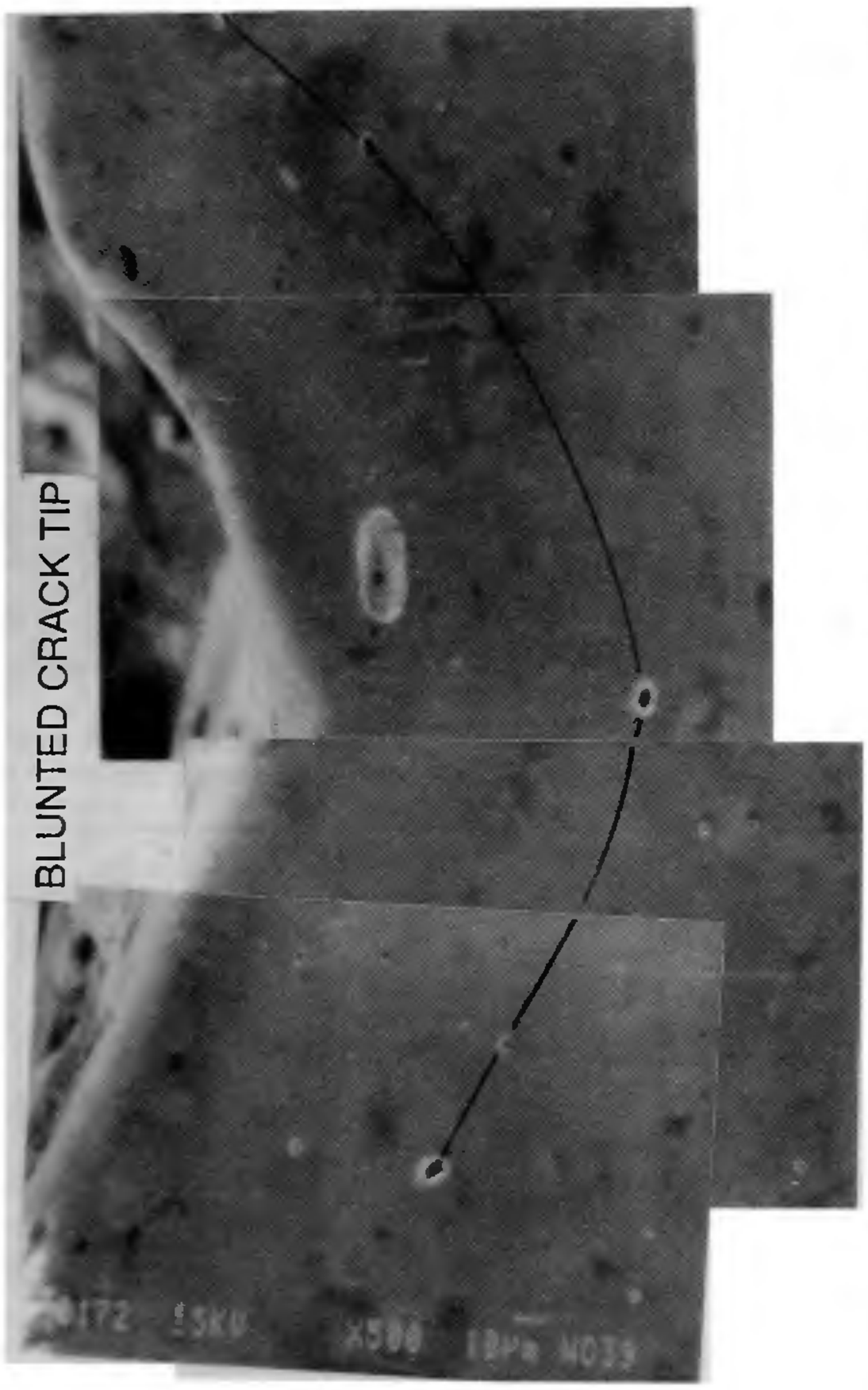

Figure 12. Scanning electron micrographs of Armco iron of 78 μm grain size showing array of parallel voids.

where σ_0 is the strength coefficient and k_y the grain size exponent. Stonesifer and Armstrong[25] proposed a relationship that correlates the critical stress intensity factor K_{Ic} with yield stress σ_y as

$$K_{Ic} = C\, r_p^{1/2}\, \sigma_y, \tag{12}$$

where r_p is the plastic zone size. Further, J_{Ic} is related to K_{Ic} as

$$J_{Ic} = K_{Ic}^2 (1-\nu^2)/E, \tag{13}$$

where ν is Poisson's ratio. The dependence of J_{Ic} on grain size is obtained by combining the three equations (11), (12) and (13) and would be given by

$$J_{Ic} = C^2 r_p \sigma_0^2/E' + (C^2 r_p \sigma_0 k_y/E')d^{1/2} + [(C^2 r_p k_y/E')d^{-1/2}]^2. \tag{14}$$

J_{Ic} measurements were made on Armco iron of varied grain size ranging from 38 to 1050 μm. The fracture toughness data[26] presented in Figure 14 reveal that J_{Ic} decreases with coarsening of grain size and follows a parabolic relation with $d^{1/2}$ as

$$J_{Ic} = 65.6 + 25.8\, d^{-1/2} + 2.5\, (d^{-1/2})^2. \tag{15}$$

Apart from validating the relation (Figure 16) we find, interestingly, occurrence of brittle cleavage at room temperature in iron specimens (precracked) of 1050 μm grain size (Figure 17). The cleavage fracture behaviour at room temperature can be explained in terms of the stress concentration

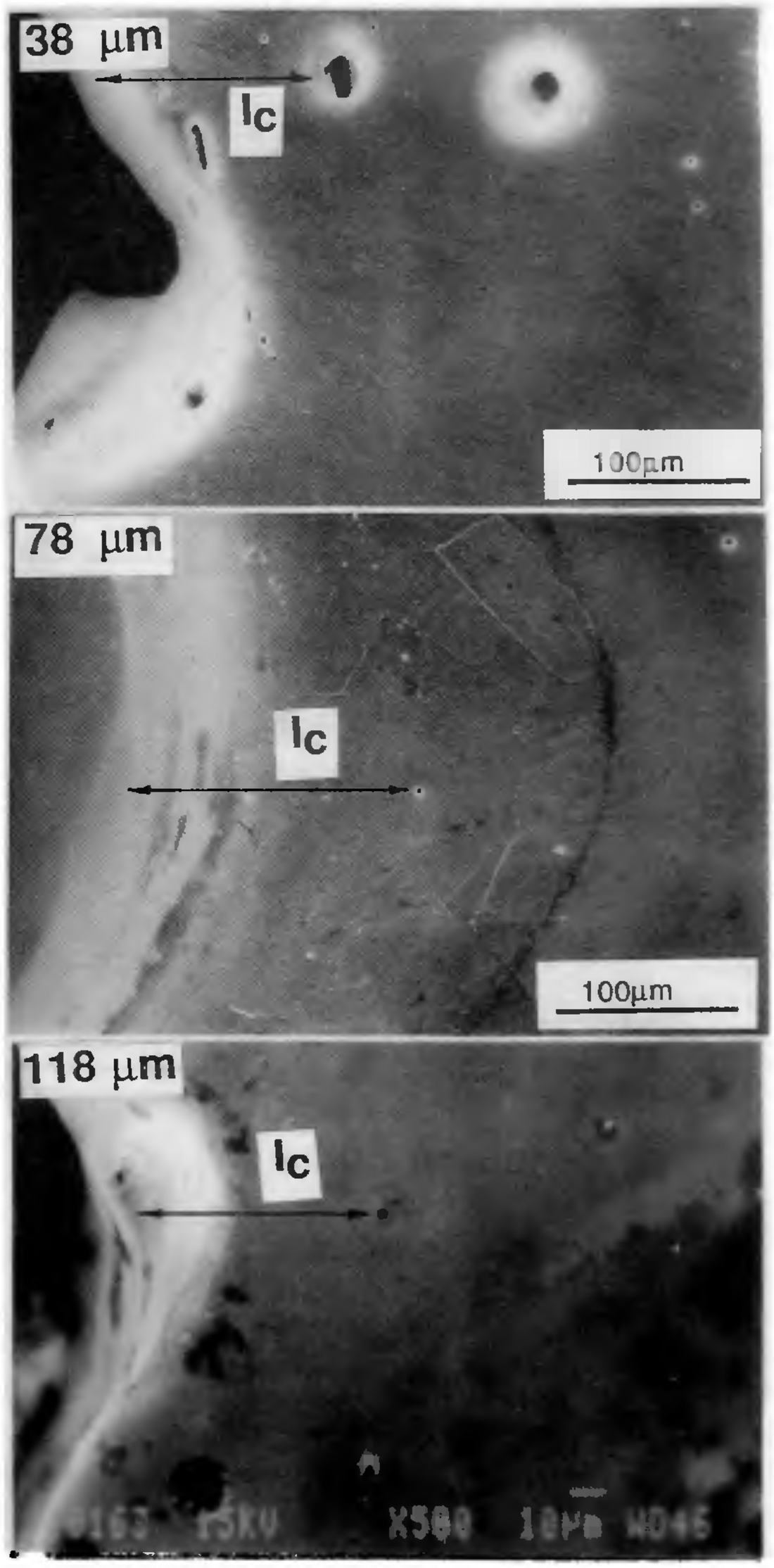

Figure 13. Scanning electron micrographs of Armco iron of varied grain size revealing characteristic distance.

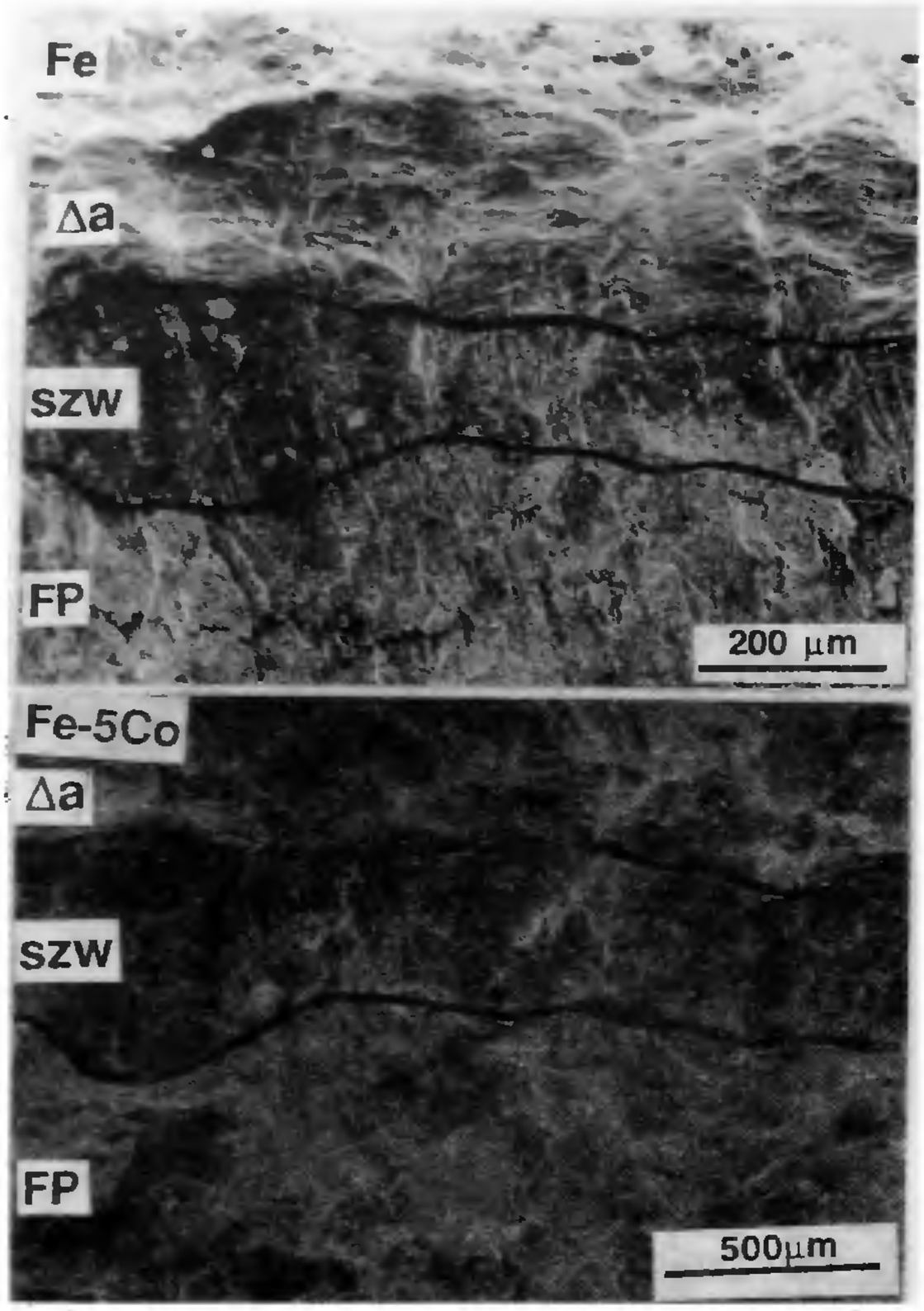

Figure 14. Scanning electron micrographs revealing critical stretch zone width for Armco iron and Fe–5Co alloy.

ahead of the crack tip attaining the level of the cleavage fracture stress and the planar slip conditions when the plastic zone confines to just about one grain[26].

Grain size variation also influences work hardening behaviour and the size of the plastic zone ahead of the crack tip. The work-hardening exponent n decreases from 0.3 to 0.255 when the grain size is varied from 38 μm to 420 μm. In a similar manner, as expected, the plastic zone size decreases with coarsening of the grain size (Figure 18). At finer grain sizes the plastic zone encompasses a greater number of grains which implies a greater energy input in overcoming the grain boundary resistance to fracturing of polycrystal grains, which explains higher values of J as grain size is decreased.

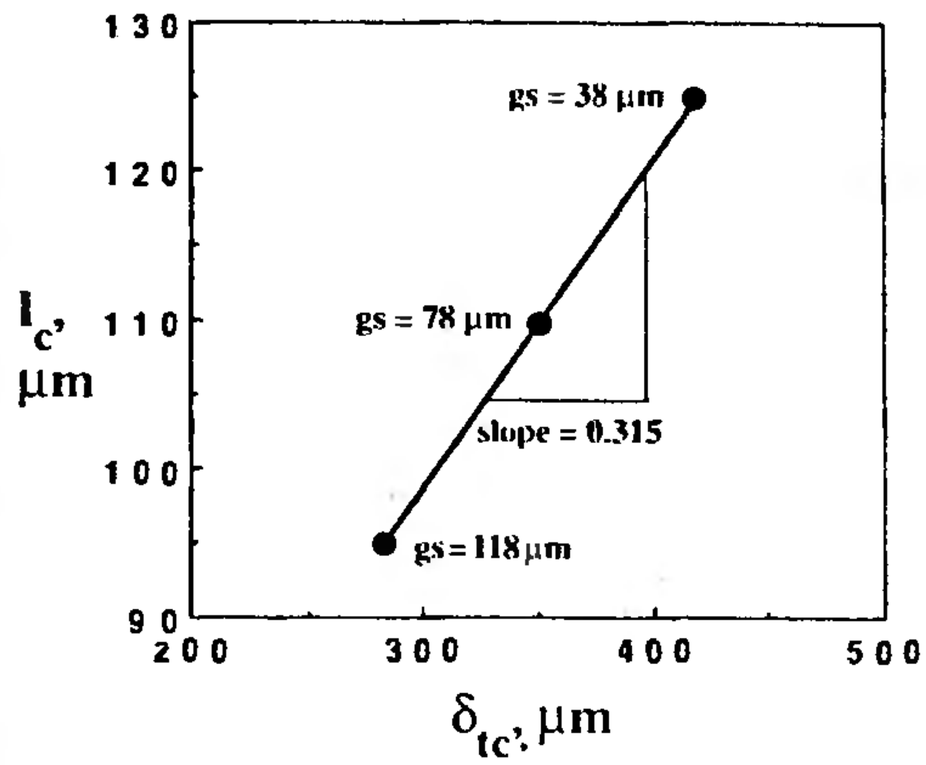

Figure 15. Variation of crack tip opening displacement δ_{tc} with characteristic distance l_c for Armco iron of varied grain size.

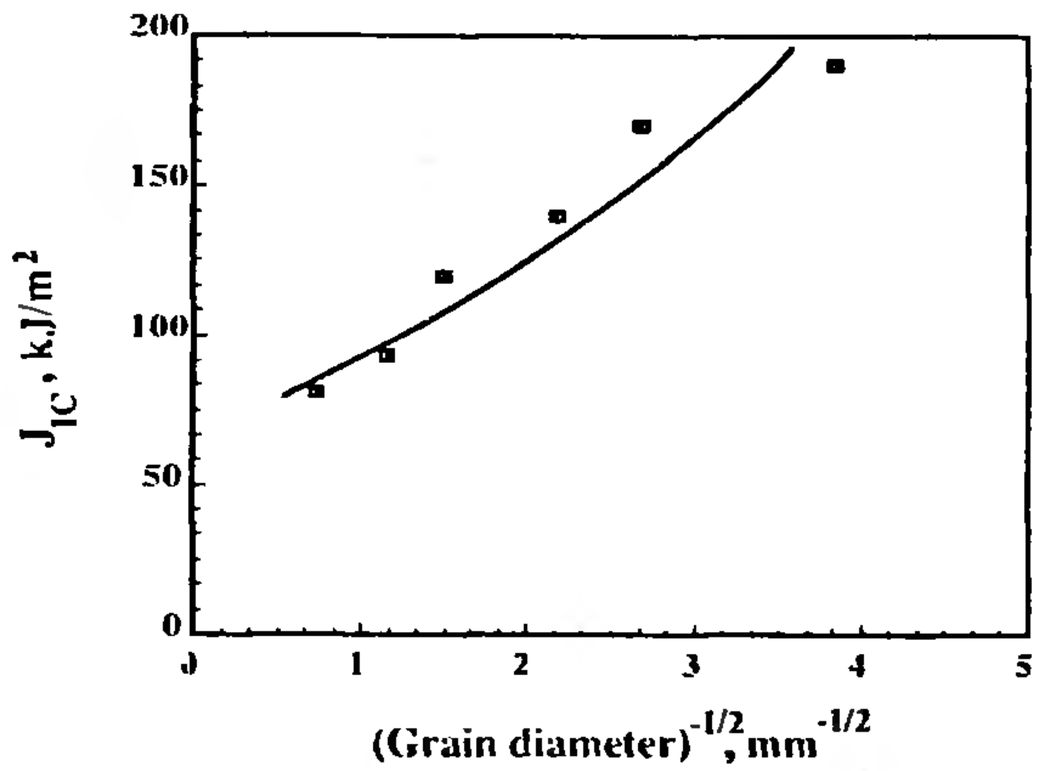

Figure 16. Variation of J_{Ic} with grain size for Armco iron.

Solute effects

Commonly used alloying elements in steels, viz. silicon, molybdenum, nickel, cobalt and chromium were chosen as solutes. Iron-based solid solution alloys, at two concentration levels in each case, were evaluated for tensile and fracture toughness properties[27].

As a prelude to examining J as a function of the solute addition, simple tensile tests were carried out (Figure 19). It is evident from Figure 19 that cobalt and chromium cause solid solution softening while molybdenum, nickel and silicon strengthen iron. Silicon has pronounced hardening effect.

Alloy softening due to cobalt was further investigated. One of the reasons for alloy softening conjectured in the literature is that cobalt as substitutional solute causes scavenging of interstitial carbon. This has been attributed to the notion that cobalt enhances thermodynamic activity of carbon in iron, which means that it reduces the

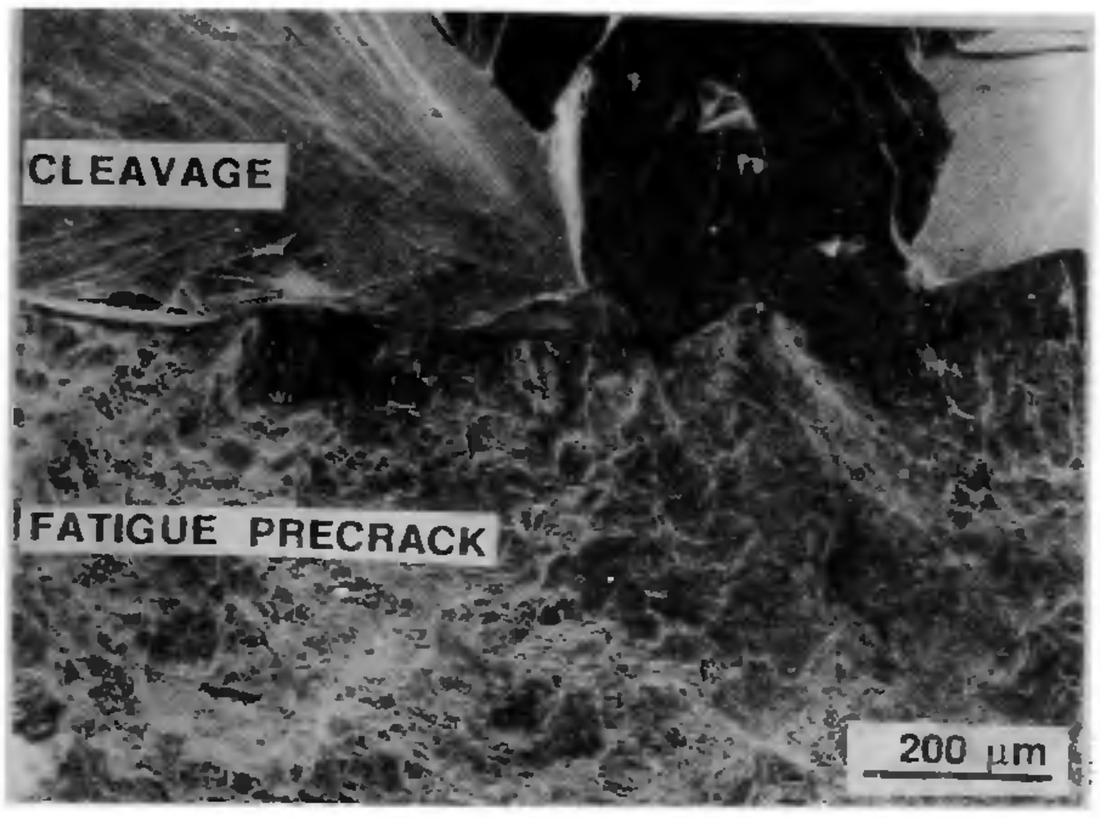

Figure 17. Scanning electron micrograph showing cleavage fracture in Armco iron of grain size 1050 μm fracture toughness tested at room temperature.

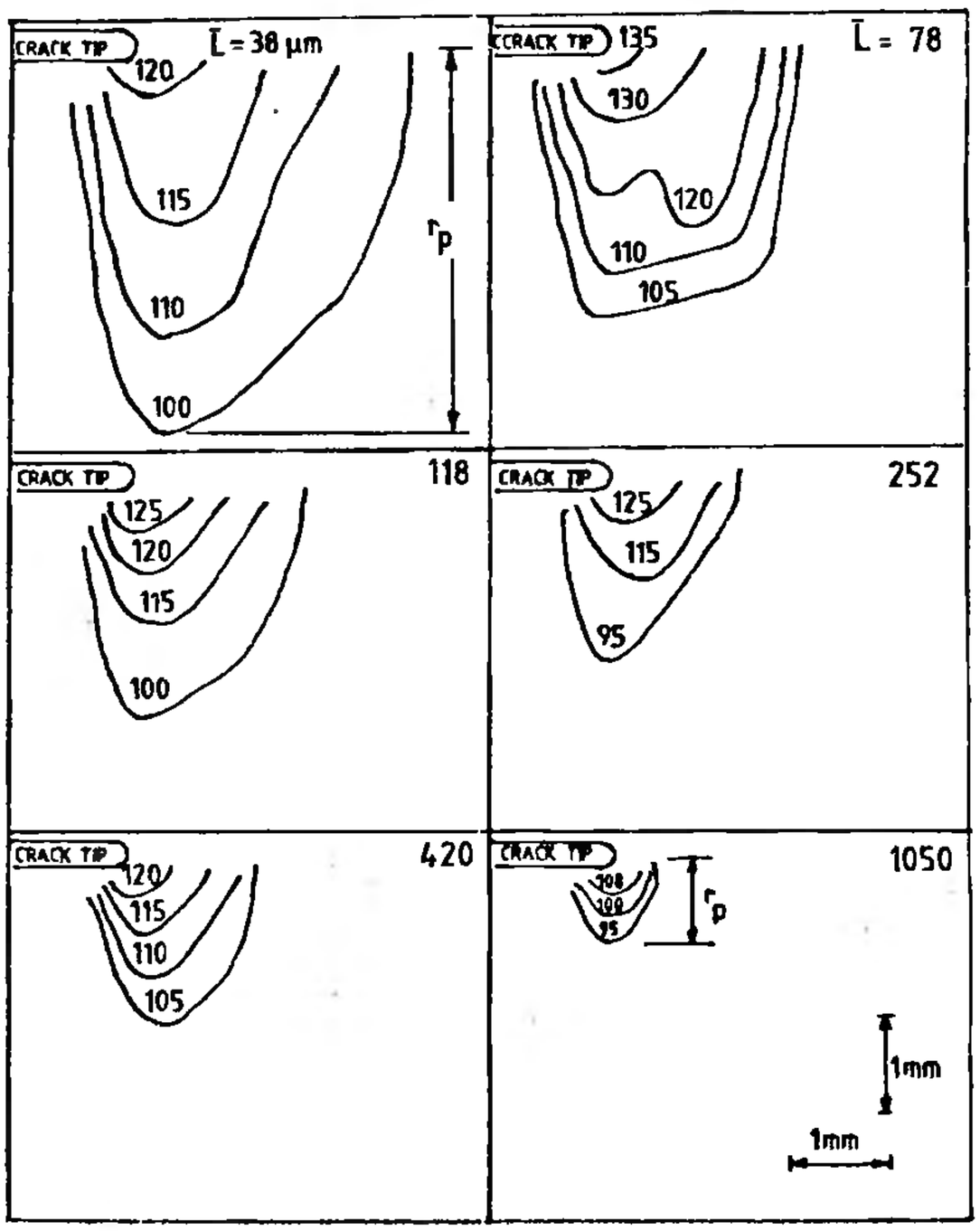

Figure 18. Microhardness profiles of Armco iron of varied grain size.

energy of carbon atom interaction with the metal atoms. We have, for the first time, obtained evidence for carbon segregation to grain boundaries through secondary ion mass spectroscopy (SIMS). Ion images for Armco iron (Figure 20 *a*, *b*) clearly indicate that the interstitial carbon is homogeneously distributed in the solution. On the

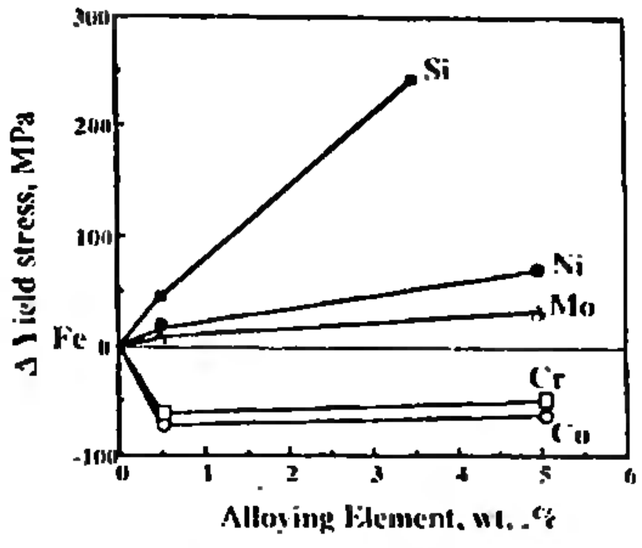

Figure 19. Change in yield stress of iron as a function of alloying element content.

other hand, C^- and CN^- ion images for Fe–5Co alloy (Figure 20 *c*, *d*) clearly reveal segregation of carbon and nitrogen at the grain boundaries.

To substantiate SIMS observations, the Hall–Petch constants were determined from yield strength data obtained over a wide range of grain size for Fe and two binary alloys Fe–0.5Co and Fe–3.5Si. The scavenging mechanism implies removal of carbon from the grain interior and its segregation to the grain boundaries. If this is operative, it should be seen from the Hall–Petch constants, namely σ_0 (a measure of friction stress resisting dislocation movement within the grain) and k_y (a measure of grain boundary strength). Figure 21 shows variation of yield stress with grain size for Fe, Fe–0.5Co and Fe–3.5Si. σ_0 and k_y values are also included in the figure. Cobalt addition causes significant reduction in σ_0 (118 MPa to 39 MPa) whereas K_y increases from 25.6 to 36.8 MPa$\sqrt{m}$. An increase in k_y with cobalt addition indicates segregation of interstitial carbon atoms to the grain boundaries as carbon is known to contribute to grain boundary cohesion in Fe. On the other hand, silicon being a strong solid solution strengthener causes, at a concentration level of 3.5 wt%, a three-fold increase in σ_0 without influencing k_y.

Fracture toughness (J_{Ic}) data for the five binary alloys are plotted as a function of alloying content (Figure 22 *a*). The notable observation is that cobalt imparts to Armco iron significant improvement in fracture toughness. On the other hand, Mo and Si have an increasing degree of deleterious effect, with the least effect observed for chromium. The marked lowering of J_{Ic} in Fe–Ni alloys is due to the effect of sulphur segregation, as explained elsewhere[27].

The increase in J_{Ic} with cobalt addition can be understood in terms of the enhanced strain hardening exponent, which is known to have a bearing on the plastic zone size around the crack tip and on micromechanisms of crack initiation. The large decrease in J_{Ic} with silicon and higher molybdenum concentration is explained on the basis of a change in fracture mode from ductile to cleavage as a result of stress concentration ahead of the crack tip reaching the cleavage fracture stress.

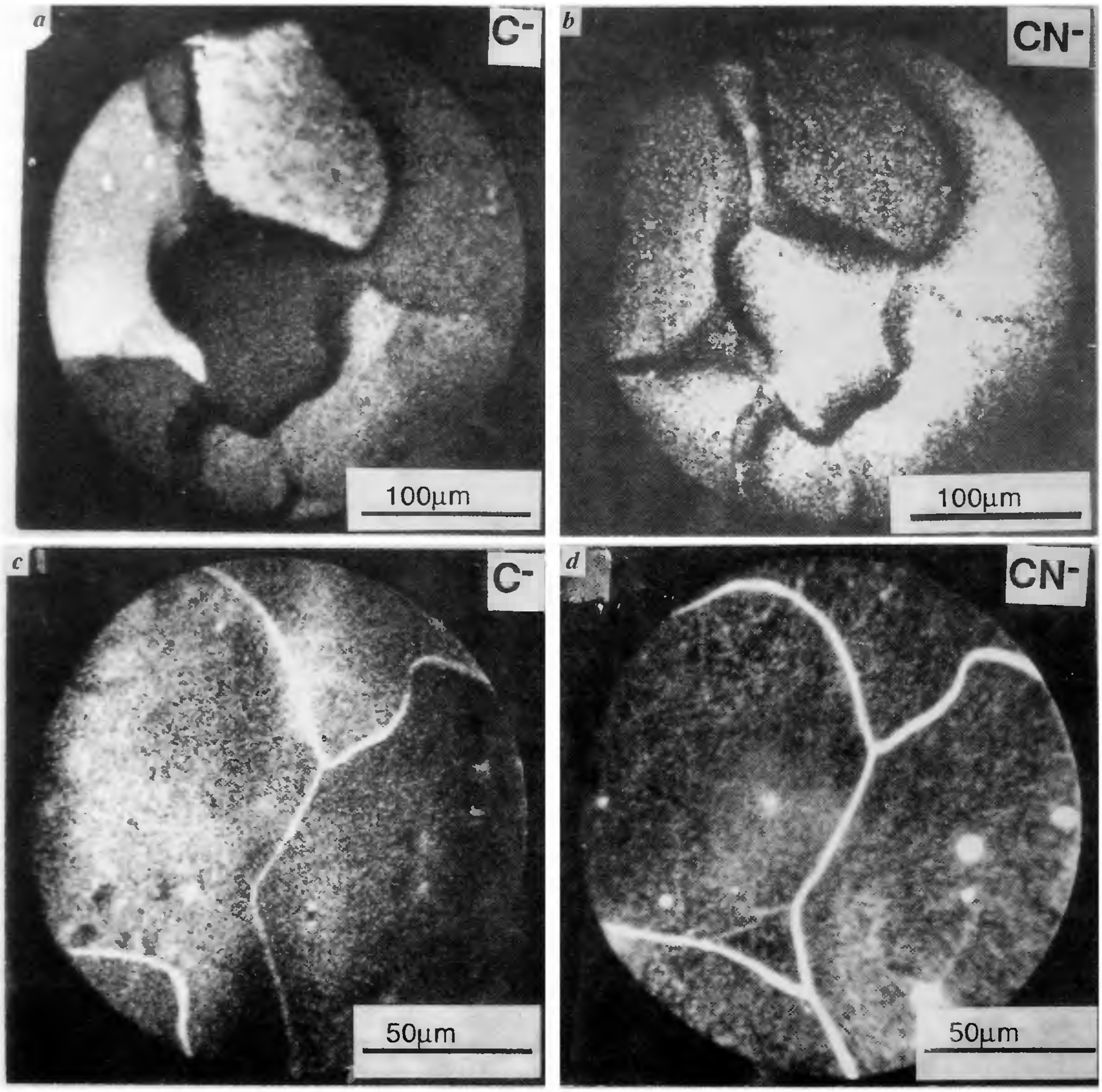

Figure 20. Secondary ion mass spectroscopy images for (*a,b*) Armco iron and (*c,d*) Fe–5Co alloy.

The influence of solute additions on the strain hardening exponent n is shown in Figure 22 *b*. A close similarity exists between the variation of J_{Ic} and n with alloying element. Of all the five elements investigated, cobalt is the only element that increases n of iron. Increased n also results in larger plastic zone size[27].

Effects of temperature

At low temperature, iron loses its fracture resistance drastically due to the onset of brittle fracture which, as is well known, is a characteristic of b.c.c. materials. Increasing the temperature from the ambient to 343 K results in a marginal increase (~ 8%) in J_{Ic} of Armco iron. A further increase in temperature is accompanied by a dramatic increase in J_{Ic} (Figure 23). A maximum of J_{Ic} (290 kJ/m^2 compared to the room temperature value of 170 kJ/m^2) was obtained at 473 K. Armco iron exhibits dynamic strain ageing (DSA) in the temperature range 383–573 K, wherein a significant increase in fracture toughness is observed[28]. The present results show that DSA is intrinsically a strengthening as well as a toughening mechanism. This should be expected from the influence of DSA on strain hardening (Figure 23).

The variation of J_{Ic} of iron as influenced by grain size, alloying element and test temperature is presented in Figure 24 as a function of strain hardening exponent n. A general tendency for J_{Ic} to increase with increasing n is evident. The effect of n is most marked with grain size. With the J_{Ic} experiments thus covering a wide range (100–300 kJ/m^2), the stage is set for the analysis of the data.

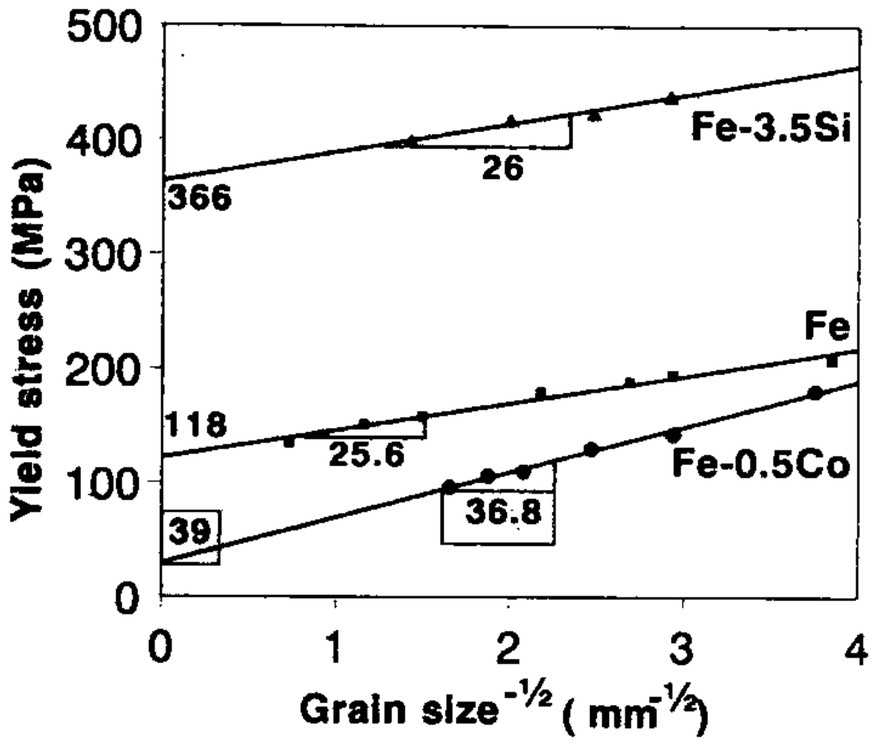

Figure 21. Variation of yield stress with grain size for Armco iron, Fe–0.5Co and Fe–3.5Si alloy.

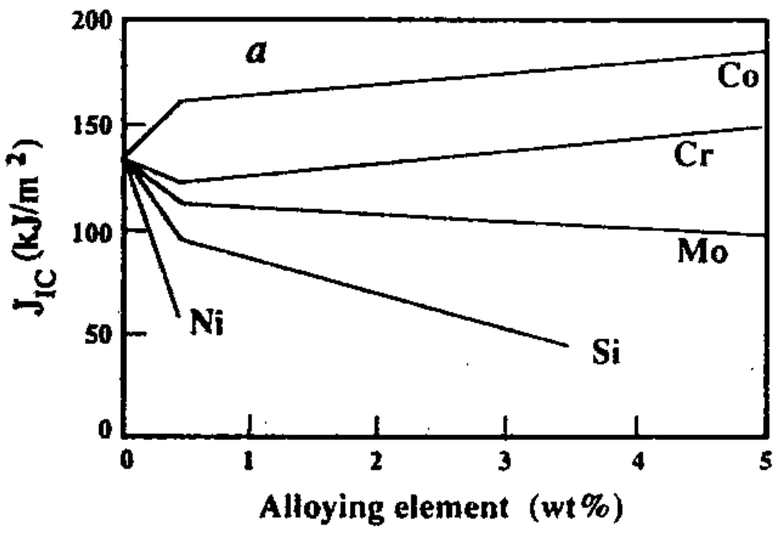

Figure 22. Variation of J_{Ic} (a) and strain hardening exponent (b) of iron with alloying element content.

Analysis of ductile fracture data

The critical strain criterion model developed by Rice and Johnson[29] and Ritchie and Thompson[19] for engineering materials, used in the analysis of our data, assumes the presence of particles. The sequence of events leading

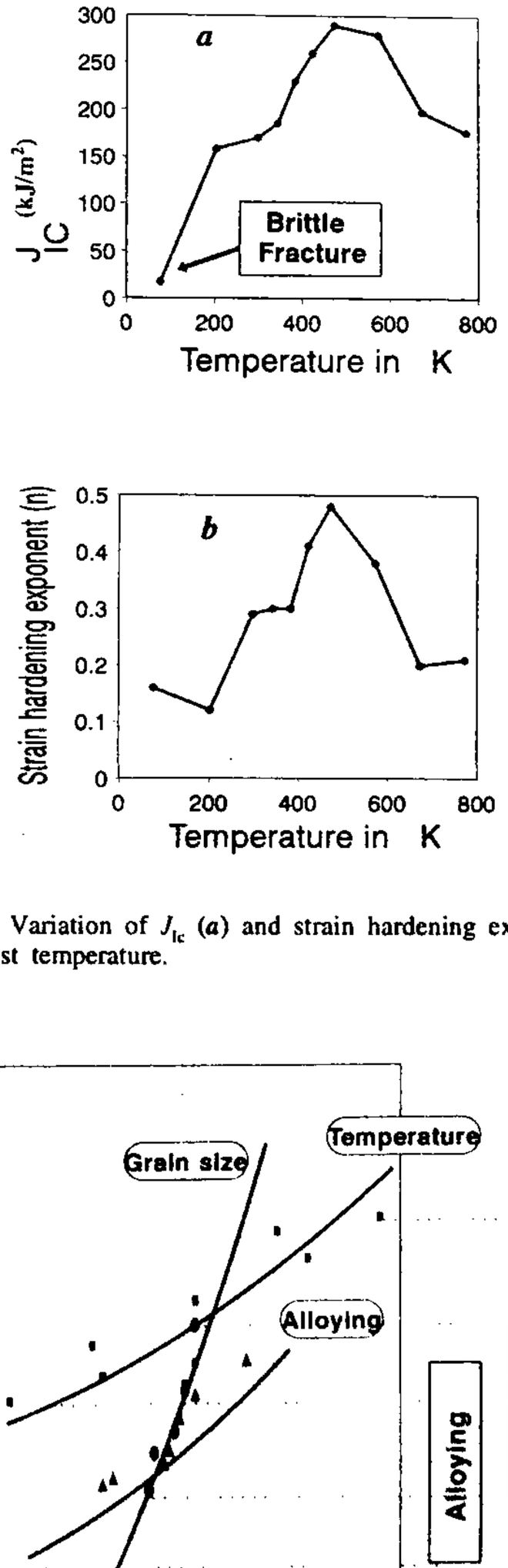

Figure 23. Variation of J_{Ic} (a) and strain hardening exponent (b) of iron with test temperature.

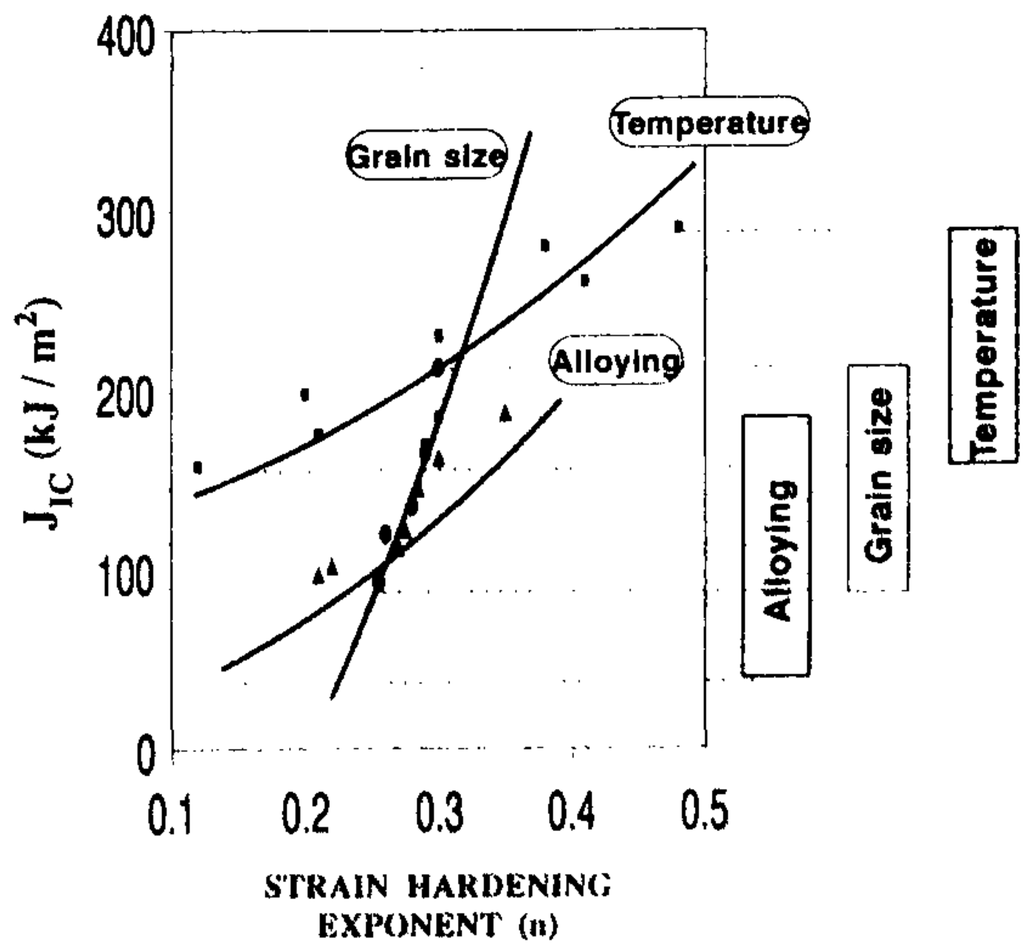

Figure 24. Variation of J_{Ic} as influenced by grain size, alloying element and temperature with strain hardening exponent.

to crack initiation is visualized as follows. As soon as the precracked sample is loaded in tension under a monotonically increasing load, extensive blunting of the crack tip occurs as has been actually seen. The crack blunting process is completed, leading to a constant stretch zone width (SZW), before void nucleation (normally at particles in most previous treatments) and growth at a characteristic distance l_c from the blunted crack tip (Figure 25). The interrelationship between J_{Ic}, the critical fracture strain ε_f and the characteristic distance l_c is given by[22,25]

$$J_{Ic} = C_1(K_H \varepsilon_f^{n+1}/n+1)\, l_c, \tag{16}$$

where

$$C_1 = I_n (n+1)/\varepsilon_{ij}. \tag{17}$$

The values of I_n and ε_{ij} for different values of n and θ have been computed by Hutchinson[22], Shih[30] and Harlin and Willis[32]. However, the extensive blunting of the crack tip that occurred in our experiments on Fe, substantially free from particles, alters the HRR stress and strain fields very near the crack tip and also the angular distribution of the function ε_{ij}. The above effects related to blunting alter C_1 and, hence, the value of C_1 obtained on the sharp crack assumption will not be appropriate in the present case.

It is to be noted that the zone ahead of the crack tip experiencing deformation also changes in size during the course of crack initiation. With reference to Figure 25, up to the point when the plastic strain (ε) ahead of the crack at l_c reaches the nucleation strain (ε_n), the strain distribution ahead of the blunted crack is given by the expression

$$\varepsilon = 2.3 \exp(-2.34\, X/\delta_t), \tag{18}$$

where X is the distance ahead of the crack tip on the crack plane ($\theta = 0$) and δ_t is the crack tip opening displacement. The material within the HRR zone extending to about $2.3\,\delta_{tc}$ from the crack tip experiences substantial plastic flow. In contrast, once void growth starts, further deformation is localized in the process zone (Figure 25).

Based on the above scenario, the energy absorbed per unit volume of the material before crack initiation, can be grouped as follows:

(i) Energy absorbed in the process zone up to nucleation of void

$$E_{nuc} = K_H \varepsilon_{nuc}^{n+1}/n+1, \tag{19}$$

where

$$\varepsilon_{nuc} = 2.3 \exp(-2.35\, l_c/\delta_{tc}). \tag{20}$$

(ii) Energy absorbed in the process zone during void growth up to its coalescence with the main crack

$$E_{grow} = \frac{K_H}{n+1} (\varepsilon_f^{n+1} - \varepsilon_{nuc}^{n+1}), \tag{21}$$

where

$$\varepsilon_f = [\ln (b l_c/a_0)/0.28] \exp(-1.5\sigma_m/\sigma) + \varepsilon_{nuc}. \tag{22}$$

(iii) The energy absorbed in the HRR zone extending to a distance of about $2.3\,\delta_{tc}$ from crack tip exclusive of the process zone

$$E_{HRR} = [K_H (2.3\,\delta_{tc} - l_c)/n+1]\, \varepsilon_{av}^{n+1}, \tag{23}$$

where

$$\varepsilon_{av} = \frac{\delta_{tc}}{2.3\,\delta_{tc} - l_c} \exp(-2.35\, l_c/\delta_{tc}) \tag{24}$$

and ε_{av} is the average plastic strain in the HRR zone exclusive of the process zone.

The J_{Ic} expression derived earlier (eq. (16)) includes only the first two energy terms E_{nuc} and E_{grow} and presumes that the energy absorbed in the HRR zone is negligible as compared with the energy absorbed/dissipated in the process zone. However, the assumption is not entirely valid as will be shown. Hence, a more accurate expression for J_{Ic} can be obtained as

$$J_{Ic} = C[E_{nuc}\, l_c + E_{grow}\, l_c + E_{pl}(2.3\,\delta_{tc} - l_c)]. \tag{25}$$

The input parameters K_H and n are obtained from tensile data ($\sigma = K_H \varepsilon^n$) and δ_{tc} from stretch zone measurements. σ_m is estimated using δ_{tc} from $\sigma_m/\sigma = 0.577\,[1 + 2 \ln (1 + 2\, l_c/\delta_{tc})]$. Reasonable values are assigned to a_0 the initial radius of the void at the time of nucleation and bl_c, the final radius of the void at which it coalesces with the main crack. l_c, the critical distance is estimated from SEM measurements.

In ductile metals, the magnitude of local strain is substantially larger and the strain distribution extends much further. From a given strain, amplification of local

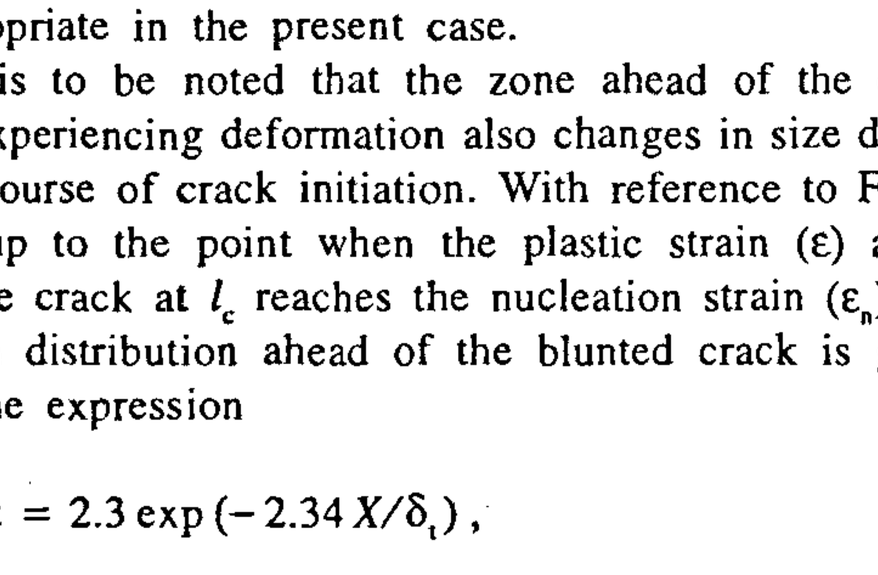

Figure 25. A schematic illustration of the plastic zone field of a blunted crack tip delineating the various zones.

flow stress is much higher on account of higher strain hardening. Energy dissipated in the plastic zone is a function of the product of local flow stress and strain. Thus, energy dissipation in HRR zone, ignored for less ductile alloys, is reckoned with in ductile metals.

Theoretically predicted J_{Ic} values are compared in Figure 26 with those derived experimentally. This includes data pertaining to alloying additions, grain size and test temperature. It is evident from Figure 26 that the proposed method estimates reasonably well (to within $\pm 15\%$) the ductile initiation fracture toughness J_{Ic} of single phase materials exhibiting a wide range of values. Our analysis[33] indicates that the assumption that energy required for crack initiation (J_{Ic}) is equal to the energy dissipated in the process zone only is not valid, at least in the case of very ductile materials, because the proportion of the total energy dissipated in the HRR zone excluding the process zone can be as high as 15 to 25% depending on the actual material.

Development of a special steel

As already described, the basic studies on the toughening behaviour of Armco iron as influenced by the alloying additions have revealed that, among the five alloying elements studied, viz. cobalt, chromium, nickel, molybdenum and silicon, cobalt imparts significant improvement in fracture toughness. An extension of these studies to Fe–C–X alloys, where X is Co or Ni, interestingly revealed that the beneficial effect of cobalt is even more pronounced in the presence of carbon (Figure 27). With a 5 wt% cobalt addition the J_{Ic} of Fe–0.2C alloy is enhanced nearly 80% while maintaining the same level of strength.

Based on the understanding developed, cobalt addition was made to the Garrison[34] NiSiCr steel to achieve further improvement in fracture toughness. A significant improvement in fracture toughness is seen (compare the bars of J_{Ic} for NiSiCr and NiSiCrCo steels in Figure 27). The accompanying loss in strength due to the addition of cobalt to the base NiSiCr steel was compensated by molybdenum addition. While molybdenum is a solid solution strengthener, the fracture toughness of Armco iron is only marginally lowered as a result of molybdenum addition, when below a certain level of concentration. To optimize the composition, melts with varying content of cobalt and molybdenum were processed and tested[35]. The strength–toughness data of NiSiCrCoMo steel thus developed fall in the upper bound range of 250 grade maraging steel (Figure 28).

Technology development of the steel was then pursued through industrial scale melts and detailed studies pertaining to formability and weldability. The attractive combination of strength and toughness observed in the laboratory melt is seen to be reproducible in the industrial scale melt (Table 3). NiSiCrCoMo steel in the softened condition can easily be rough machined before finally subjecting to hardening and tempering treatment in order to develop an optimum combination of strength and fracture toughness. The steel in the softened condition also possesses good formability. Weld parameters have also been established. With base steel as filler (which had to be duly processed), 95% or better weld efficiency in terms of yield strength as well as fracture toughness is achievable in the weld and heat treated condition.

The newly developed NiSiCrCoMo steel obviously provides significant cost saving once we consider the fact that this steel possesses a maximum alloy content of ~ 7% whereas the alloying content of maraging 250

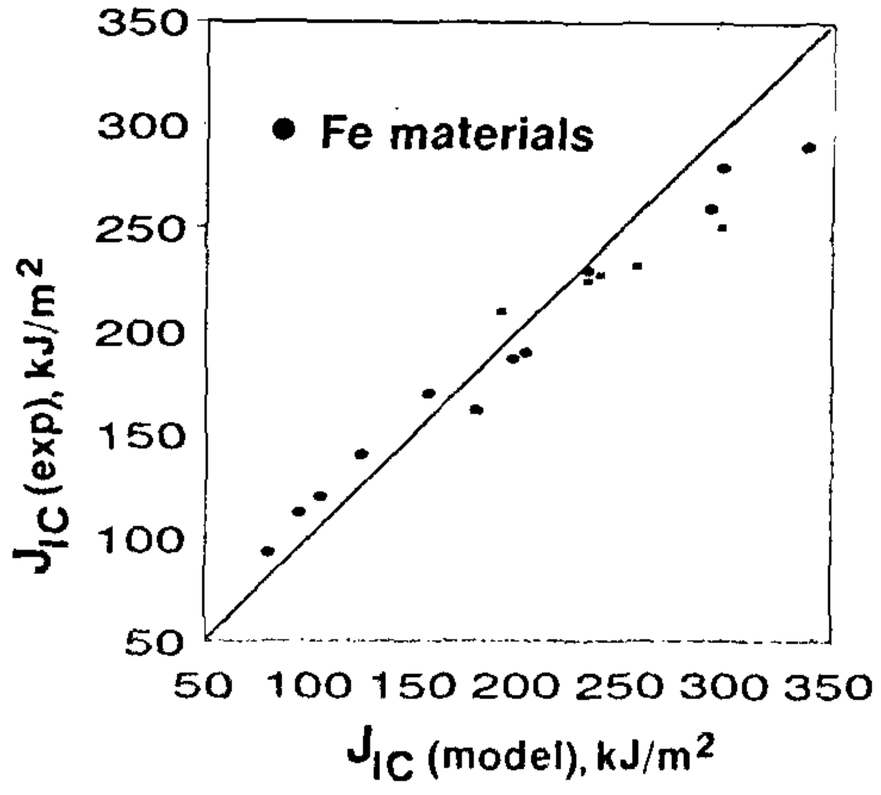

Figure 26. A comparison of J_{Ic} evaluated experimentally with J_{Ic} predicted by analysis.

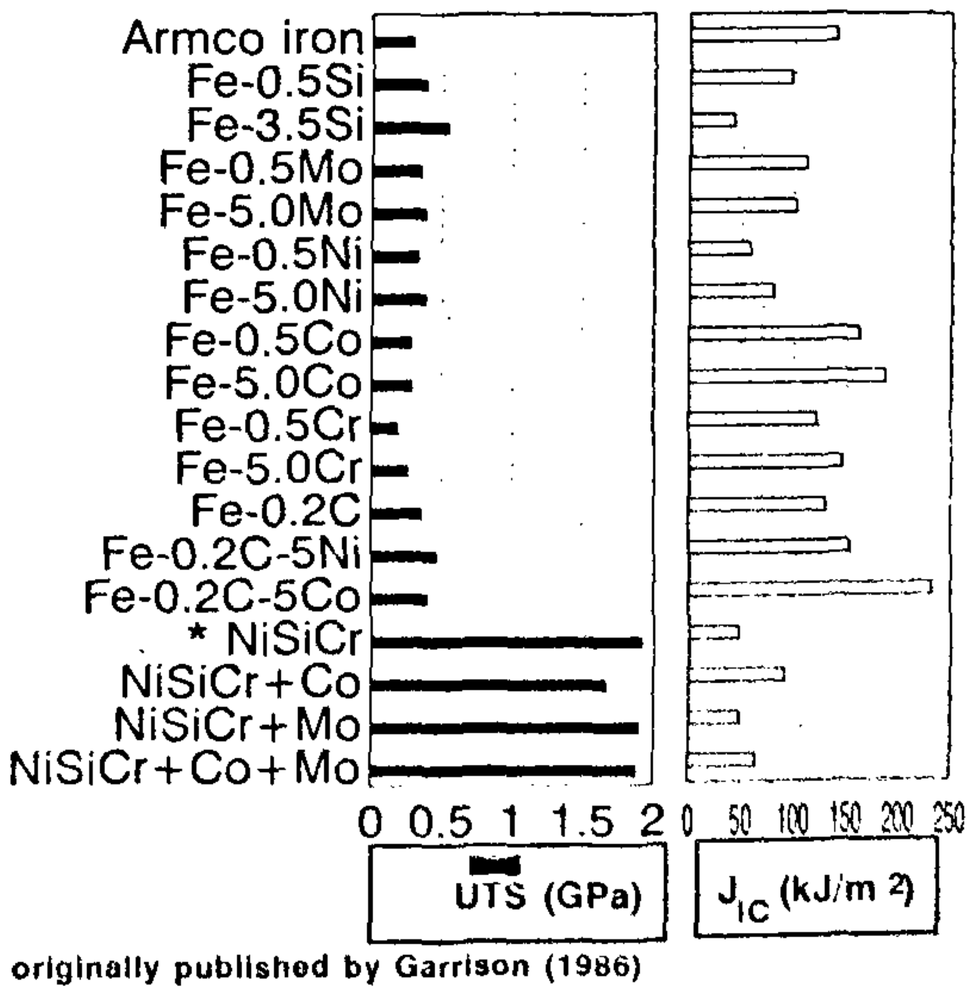

Figure 27. Histograms showing strength and toughness variations of iron-based solid solutions, Fe–C–X alloys and NiSiCr-based steels.

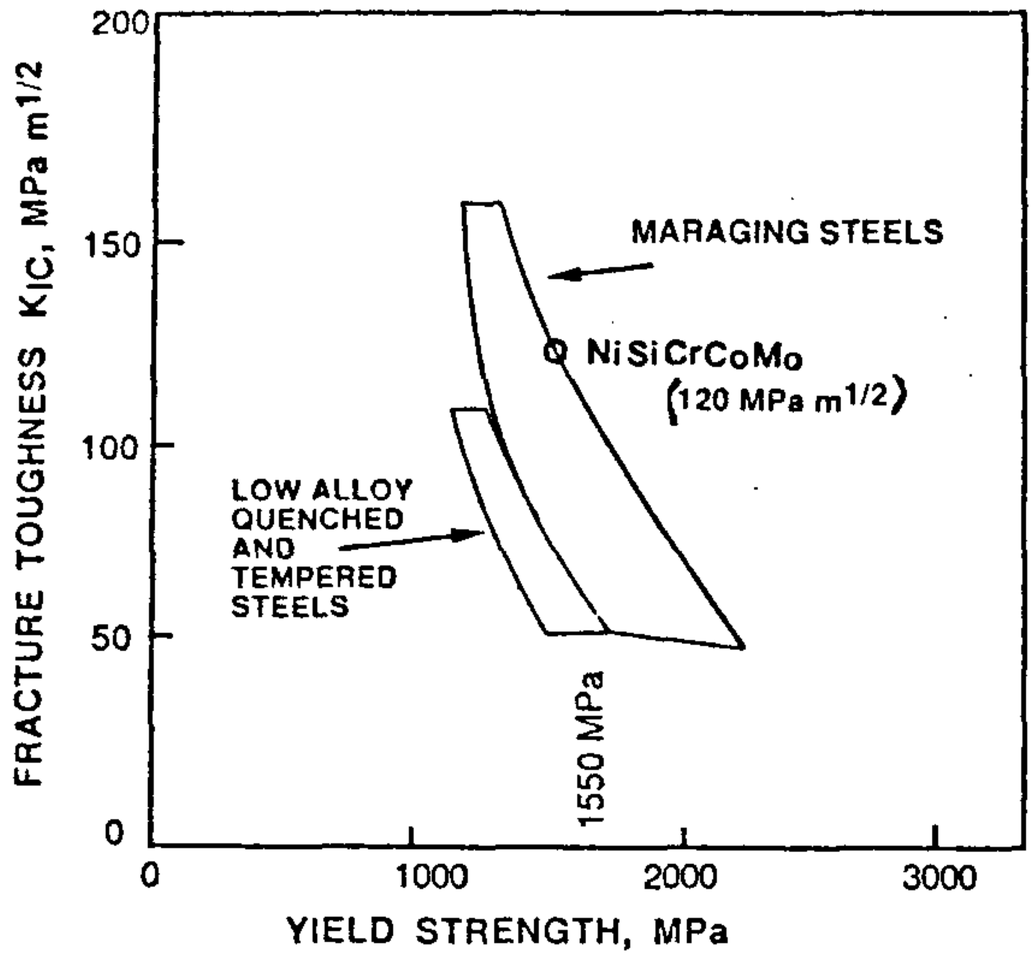

Figure 28. Strength–toughness data for NiSiCrCoMo steel superimposed onto the bands for maraging steel and low alloy quenched and tempered steels.

Table 3. Reproducibility of properties in tonnage melts

Property	Lab-scale melt (30 kg)	Industrial melt (5000 kg)
Yield stress (MPa)	1530	1575
UTS (MPa)	1890	1950
Elongation (%)	14	13.6
K_{Ic} (MPa$\sqrt{m}$)	120	90–100

grade steel is in excess of 30% (ref. 10). That low-alloy steels generally possess superior biaxial strength[36] is a feature worthy of note. The use of the NiSiCrCoMo steel for various structural applications can now be considered.

1. Griffith, A. A., *Philos. Trans. R. Soc. London*, 1920, **A221**, 163.
2. Orowan, E., *Rep. Progr. Phys.*, 1948, **XII**, 185.
3. Irwin, G. R., *Fracturing of Metals*, American Society for Metals, Cleveland, 1948, p. 147.
4. Mott, N. F., *Engineering*, 1948, **165**, 16.
5. Irwin, G. R. and Kies, J. A., *Welding J. Res. Suppl.*, 1952, **31**, 95s.
6. Irwin, G. R., *J. Appl. Mech.*, 1957, **24**, 361.
7. Rice, J. R., *Fracture – An Advanced Treatise* (ed. Liebowitz, H.), Academic Press, New York, 1968, vol. II, p. 191.
8. Begley, J. A. and Landes, J. D., *Fracture Toughness, Part II*, ASTM STP 514, American Society for Testing and Materials, Philadelphia, 1972, p. 1.
9. Pickering, F. B., *Physical Metallurgy and Design of Steels*, Applied Science Publishers, London, 1978.
10. *Source Book on Maraging Steels*, American Society for Metals, Metals Park, Ohio, 1979.
11. ASTM E813-81, *Standard Method of J_{Ic} – A Measure of Fracture Toughness*, Annual Book of ASTM Standards, American Society for Testing and Materials, Metals Park, Ohio, Section 3, 1986, p. 768.
12. Srinivas, M., Malakondaiah, G. and Rama Rao, P., *Eng. Fracture Mechanics*, 1987, **28**, 561.
13. Mills, W. J., *J. Test. Eval.*, 1981, **9**, 56.
14. Eberhart, M. E., Latanision, R. M. and Johnson, K. H., *Acta Metall.*, 1985, **33**, 1783.
15. Garrison, Jr. W. M., *Scr. Metall.*, 1984, **18**, 583.
16. Lin, T., Evans, A. G. and Ritchie, R. O., *Acta Metall.*, 1986, **34**, 2205.
17. Lin, T., Evans, A. G. and Ritchie, R. O., *J. Mech. Phys. Solids*, 1986, **34**, 477.
18. Neville, D. J., *J. Mech. Phys. Solids*, 1988, **36**, 443.
19. Ritchie, R. O. and Thompson, A. W., *Metall. Trans.*, 1985, **A16**, 233.
20. Knott, J. F., *Metal Sci.*, 1980, **16**, 327.
21. Argon, A. S., Im, J. and Sofoglu, R., *Metall. Trans.*, 1975, **A6**, 825.
22. Hutchinson, J. W., *J. Mech. Phys. Solids*, 1988, **16**, 1.
23. Rice, R. J. and Rosengren, G. R., *J. Mech. Phys. Solids*, 1968, **16**, 1–12.
24. Robinson, J. N. and Tetelman, A. S., *Engg. Fract. Mech.*, 1976, **8**, 301.
25. Stonesifer, F. R. and Armstrong, R. W., *Advances in Research on the Strength and Fracture of Materials, The Physical Metallurgy of Fracture* (ed. Taplin, D. M. R.), Pergamon, Oxford, 1977, vol. 2A, p. 1.
26. Srinivas, M., Malakondaiah, G., Armstrong, R. W. and Rama Rao, P., *Acta Metall. Mater.*, 1991, **39**, 807.
27. Srinivas, M., Malakondaiah, G. and Rama Rao, P., *Proc. R. Soc. London*, 1994, **A447**, 223.
28. Srinivas, M., Malakondaiah, G. and Rama Rao, P., *Acta Metall. Mater.*, 1993, **41**, 1301.
29. Rice, J. R. and Johnson, M. A., *Inelastic Behaviour of Solids* (eds Kannien, M. F., Adler, W. F., Rosenfield, A. R. and Jaffee, R. I.), McGraw Hill, New York, 1970, p. 641.
30. Shih, C. F., Brown University Report No. MRL E-147, Providence, 1983.
31. Lin, T., Evans, A. G. and Ritchie, R. O., *Metall. Trans.*, 1987, **A184**, 641.
32. Harlin, G. and Willis, J. R., *Proc. R. Soc. London*, 1988, **A415**, 197.
33. Srinivas, M., Sundararajan, G., Malakondaiah, G. and Rama Rao, P., *Proc. R. Soc. London*, 1994, **A447**, 237.
34. Garrison Jr. W. M., *Metall. Trans.*, 1986, **A17**, 669.
35. Malakondaiah, G., Srinivas, M., Marthanda Murthy, J. and Rama Rao, P., *Bull. Mater. Sci.*, 1994, **17**, 73.
36. Bhat, G. K., in *High-Strength Steels for the Missile Industry* (ed. Sumsion, H. T.), American Society for Metals, Metals Park, Ohio, USA, 1961, p. 153.
37. Ritchie, R. O., Knott, J. F. and Rice, J. R., *J. Mech. Phys. Solids*, 1973, **21**, 395.
38. Curry, D. A., *Metal Sci.*, 1980, **16**, 319.

ACKNOWLEDGEMENTS. The presentation is based on the work of my colleagues Dr G. Malakondaiah, Dr M. Srinivas and Shri J. Marthanda Murthy of DMRL, the association with whom has been so rewarding. I thank Dr G. Sundararajan for his participation in and contribution to the analysis of fracture data. The cooperation of several people of DMRL, encouragement and support of the Director Shri S. L. N. Acharyulu are gratefully acknowledged. For production technology aspects of the steel, we owe a debt of gratitude to MIDHANI, a Special Alloys plant at Hyderabad and their Chairman Shri R. K. Mahapatra.